Ion Charge State Distribution in a Laser Produced Bounded Plasma

A dissertation submitted in partial fulfillment
of the requirements for the degree of
PhD in Electronics and Electrical Engineering

Graduate School of Science and Engineering
Doshisha University

Glynnnis Mae Q. Saquilayan

September 2017

Synopsis

Laser ion sources have been known to produce a wide variety of ions including highly charged states through the laser ablation of solid materials. Depending on the laser irradiation conditions, the plasma parameters can be controlled to yield the desired species and charge state of positive ions. For the case of cluster formation, as the plasma expands adiabatically, the possibility of collisions as the ions drift outward to space are relatively low. To increase the collision rate and also the probability of producing clusters, the concept of geometric constriction to the expanding plasma led to the design of a new type of laser ion source that utilizes a hollow cylinder laser target for spatial boundary conditions.

In the study, the development of the laser ion source was investigated for a laser produced spatially bound plasma and the production of cluster ions. The unique geometry of the laser target was designed to have a hollow cylindrical structure where the plasma is ignited inside the narrow volume. The study clarified the difference in the plasma dynamics of the laser ion source operation using the hollow cylinder target as the plasma was allowed to interact with the atoms on the surface and dissipate the kinetic energies through various collisional mechanisms. The proposed scheme, aiming to produce a low plasma temperature condition, was observed to increase the probability for agglomeration and generated cluster ions.

This dissertation is composed of 7 chapters that discusses the different stages of development of the hollow cylinder target laser ion source; from the prototype design

demonstrating the principle dynamics of the plasma to an improved system configuration along with the mass analysis of the produced ions species.

The first chapter gives a brief background on the laser ion source development, its applications to particle accelerators and the different research projects to improve the ion source performance. The motivations and objectives of the study are explained including the outline of the research work. The physics of laser produced plasmas were described in the second chapter. An overview on the concepts on laser ablation, the different stages of its formation and expansion, are elaborated. An analysis of the laser produced plasma using a planar aluminum target is included in the chapter. This serves as a reference for the basic configuration of a laser ablation experiment.

The third chapter demonstrates the initial operation of the prototype system with the hollow cylinder laser target. From the high speed camera images, a luminous cloud inside the hollow target was observed during laser irradiation. The bright glow expanded towards the adjacent wall from the laser irradiated spot and building up pressure inside the small volume to enhance the collision rate. The Faraday cup measurements of the time-of-flight of the plasma pulse detected an electron burst in the onset of the signal followed by the positive distribution that corresponds to the produced ions with increasing magnitudes for more intense laser power densities. Plasma diagnostic experiments on the laser produced plasma is discussed in chapter four. The optical emission spectra of the plasma is obtained for an aluminum and graphite laser target. Low charge state ions are detected from the aluminum target but the graphite target showed charge states of up to +3. A continuum was observed in the emission spectra for both target materials indicating a thermalized state with an estimated temperature of below 1 eV. This low temperature characteristic is also

detected in the Langmuir probe experiment of the graphite target where the electron temperature was calculated to be 0.48 eV.

After the initial tests on the prototype system, performance issues on stability and laser target lifetime needed to be resolved and was discussed in chapter five. A rotating mechanism to the laser target operation employed to disribute the erosion on the inner walls of the cylinder. Time-evolution experiments showed the maximum ion current measured for the stationary graphite target was reduced to 10% after an hour of the continuous system operation while the rotating the target resulted to a steady ion current for the whole duration. With the stable operation of the system, the next chapter discusses the ion mass separation experiments for the aluminum and graphite targets used in the ion source. Two kinds of ion analysis experiments were conducted; ion extraction coupled to a time-of-flight analysis and a 90° electrostatic ion analyzer. The ion extraction signals that correspond to cluster ions were detected with small fullerites of C_{24} and C_{36} for the graphite target and large aluminum clusters of Al_{20} and Al_{52} were identified from the mass analysis. Using the graphite target for the electrostatic ion analyzer, the ion composition in a single plasma pulse was found to be dominated by low charge state ions with an abundance of C^{+1} and C^{+2} ions.

The conclusion is found in chapter 7 where the main results, a comparison between the hollow cylinder target and a planar target laser ion source operation, and also future work and recommendations are presented.

Acknowledgement

The completion of this research has been possible through the guidance and assistance of many scientists and researchers. I would like to express my deepest gratitude to everyone for their support.

First, I would like to thank my supervisor, Professor Motoi Wada of Doshisha University. I began my research with little knowledge and experience but finished my three years with even more questions than I started with. I have learned more things from him than I ever will from reading papers and textbooks. This research would never have been possible without his guidance.

I would like to express my gratitude to Dr. Masahiro Okamura of Brookhaven National Laboratory. As a young researcher who still has a lifetime left to learn, I am very grateful for the opportunity to visit his laboratory and join the experiments in his research group.

I would like to thank Dr. Mamiko Sasao for her continued support from the beginning up until the completion of my doctorate degree. Her encouragement has helped a lot during my stay in Japan.

I would also like to thank Dr. Takeshi Kanesue, Dr. Shunsuke Ikeda and Dr. Edward Beebe of Brookhaven National Laboratory for their guidance during my short stay in their laboratory. I have learned a lot from our fruitful discussions and I am very grateful.

I would like to express my appreciation to all members of the Plasma Physics Laboratory in Doshisha University, both old and new, for their warm company and for creating a conducive enviroment to do research. Being able to work alongside talented people has drove me to strive harder in my research.

I would also like to acknowledge the Global Resource Management Program of Doshisha University for allowing me to be a part of a unique doctorate program. I have gained a broader perspective of the world aside from my specialization in science. I would like to express my gratitude for the financial support I have received.

Finally, I would like to thank my parents and friends for all the encouragement and support I have received during my stay in the university.

Table of Contents

List of Tables

List of Figures

Chapter 1

Introduction

"The scientist is motivated primarily by curiosity and a desire for truth."

-Irving Langmuir

1.1 Overview

This research study presents a new type of laser ion source operated with spatial boundary conditions for the generation of cluster type ions. Utilizing a novel design of a hollow cylinder for the laser target, the formation of plasma inside a narrow volume was demonstrated for the first time. The collision mechanisms induced by the plasma interacting with the atoms on the surface of the inner wall will lead to sputtering, reflection and various collisional mechanisms which will dissipate of the kinetic energy of the incident charged particles. Although the dynamics of laser produced plasmas in a cylindrical structure has not been formally established, the principle of operation is presented in order to understand its variation to a conventional configuration of a planar target laser ion source.

With the technological advancement of lasers, it has been possible to generate a volume of high energy density through pulsed beams. The application of these powerful

lasers to the laser ablation of solids has experienced a widespread in many research areas such as materials processing, fabrication of nanostructures and even as ion sources for particle acceleration. Directing the laser onto a solid surface forms a dense plasma containing multiply charged ions needing only minimal components. This ease in operation has led to the development of laser ion sources utilizing the principle of laser ablation.

Research in laser ion sources dates back to late 60's where highly stripped ions from laser-produced plasmas reached up to charge states of +20.[1] As the plasma is generated from the irradiation of solid materials, the incident laser energy is proportional to the ion charge state distribution. In addition, the composition of the target material also translates to the ion species produced in the plasma. By changing the laser target to yield various kinds of ions, the versatility of the ion selection can be operated with faster tuning and calibration by conditioning the laser parameters. Despite the limitation of the ion source to solid targets, the production of ions of gaseous elements were tested through the laser ablation on solidified gases.[2-3] This technique permitted the ion production of non-solid materials in the laser ion source. Aside from the different ion species, the laser ion source is capable of providing multiply charged ions. Studies on coupling the ion source to different accelerators such as radio-frequency quadrulopes and other linear accelerators have been investigated for the application to particle physics.[4-6] Aiming to extend the plasma pulse width, studies were made to control the plasma shape through the use of external magnetic fields [7-8] and even using double laser systems.[9] With the ability of the laser ion source to also provide singly charged ions by lowering the laser power conditions, it has been coupled to charge breeders as the primary source of ions to efficiently increase the ion charge states.[10]

1.2 Significance of the Study

The ability to manipulate an integral part of the physical world will subsequently lead to the creation of many disciplines with technologies based on that fundamental concept. Scientific knowledge encompasses all aspects in the universe and this accentuates the need for a broader mindset; not to limit perspectives on a specific field but to start the avalanche in an interdisciplinary scale.

The knowledge acquired through developing an ion source system is deemed one of the primary skill sets upon entering a research institution on fundamental sciences. For scientists and researchers, a collective effort is needed to advance a step to progress with each having a role to fulfill. World-renowned institutes such as the National Institute for Fusion Science and Culham Centre for Fusion Energy gave valuable insights on creating a platform for engineers and scientists to apply their knowledge for the developing the field of fusion sciences. Research complex such as the Rutherford Appleton Laboratory, Japan Proton Accelerator Research Complex and Brookhaven National Laboratory operates with large scale facilities each with a specific specialization in innovation and fundamental sciences. These institutions encourage and supports scientific breakthroughs and are excellent models for establishing a research center.

Technological advancements in the world are pioneered by the extent and quality of fundamental research that may appear to be a butterfly effect which affects the dynamic systems of the society. Despite often being percieved as irrelevant by the public eye in developing countries, the activities of research institutions drive the technological innovations to universities, industries and even government agencies leading to economic impacts to the society. Having the opportunity to visit and learn

the operation of large scale research facilities with multicultural backgrounds in different countries creates a wider perception in organizing an institution for discovery. The insights brought from learning the operation of major research institutions and from the qualities as a scientist will be an invaluable asset to support developing countries towards the establishment of facilities and to become one of the forefronts in scientific progress.

1.3 Objectives and Motivations

Laser ion sources have been known to produce high charge state ions through a simple configuration and with high current intensities depending on the target material and the laser beam parameters. Studies have been made by applying constraints to control the laser produced plasma by adjusting the laser irradiation conditions and external magnetic fields to influence the shape of the plasma. Motivated by the research on manipulating the plasma plume properties, a different kind of laser ion source was developed which demonstrates a geometric constriction to the expanding plasma. A design for a new structure for the laser target was conceptualized. The main objective of the study is to produce a low plasma temperature condition to the laser ion source by introducing various collisional mechanisms. Achieving a low temperature condition will increase the probability of producing low energy ions and the agglomeration of neutral atoms to form clusters. The development of a laser ion source operating with the spatial constriction of the plasma can lead to exciting possibilities in many areas of ion source development.

1.4 Organization

The development of the hollow cylinder target laser ion source is explained in several stages starting with the prototype device up to an improved system for more stable operation. Compilation of the experiments are presented starting from the physics of laser produced plasmas, the prototype design for the laser ion source, plasma diagnostics, rotating hollow cylinder target laser ion source, mass spectrometry of the laser produced plasma and finally the conclusion.

A background on the physics and useful concepts on laser produced plasmas are explained in chapter 2. The different stages that exist in laser ablation; vaporization of atoms, formation of plasma and the expansion dynamics. These are discussed to explain the concepts before working on the laser ion source development. A laser ablation experiment using a planar aluminum target is also included as it will serve as a reference for the upcoming chapters that operates with a non-planar laser target design.

In chapter 3, the prototype system and initial experiments using the hollow cylnder target is discussed. The operation of the laser ion source was demonstrated for the first time and together with the plasma diagnostics using a high speed camera and a Faraday cup assemlby. A more detailed study on the plasma is covered in chapter 4 where different diagnostic techniques were applied to the laser produced plasma. Optical diagnostics, probe signal and Langmuir probe experiments were performed giving more details on the plasma characteristics and the generated ion species. This summarizes the assessment on the prototype laser ion source system.

With the observation from the experiments on the laser ion source, modifications were made to improve the signal stability and laser target lifetime during operation. A

rotating mechanism was designed for the system with the purpose of continuous operation and this was presented in chapter 5. The performace of the ion source was tested for its stability and the time-evolution of the ion signals were analyzed to verify the improvement brought by the addition of the rotating mechanism.

In developing an ion source, it is important to test the stability, intensity and also the ion species generated in the system. In chapter 6, the mass separation of the ions were discussed for the two experiments conducted. The ions generated using an aluminum and graphite laser target were analyzed which is essential to the possible technological appplications of the system. Lastly, the final chapter is the conclusion of the main results which is followed future work and recommendations.

Chapter 2

Physics of Laser Produced Plasma

"I can't tell you what it really is, I can only tell you what it feels like."

-Marshall Bruce Mathers III

2.1 Introduction

Given the many applications of laser ablation, the plasma formed through the intense irradiation of lasers has attracted research in different fields of science. The simplicity of its concept that basically requires a laser and a solid target to form a dense plasma led to applications in materials science for functional film formation and heavy ion sources for particle acceleration.[11-13] Fundamental studies have been conducted to give a better interpretation on the plasma ignition process and the stages of the self-extracting plasma. As the laser technology progresses, lasers have become capable of delivering a wide range of photon energies, temporal distribution and also wavelengths. The intense beams from high power pulsed laser systems have assisted in the widespread of research sustaining the investigations on the fundamental principles of laser ablation, experimental methods as well as establishing the groundwork to comprehend the physics behind it.

With the objective to develop a laser ion source for low energy ion production, understanding the physical concepts behind the formation of plasma through intense laser irradiation and the mechanisms for generating low energy ions will help the design process to work towards the research objective. In this chapter, a brief background on laser ablation will be discussed, the laser-matter and laser-plasma interaction that leads to the dense plasma formation, and the different time regimes of the plasma expansion process. It is important to review the basic concepts to aid the analysis of diagnostic experiments and provide insights to some of the observed phenomenon in the later chapters.

2.2 Laser Ablation

When a high intensity laser beam is directed on a solid surface, it undergoes different phase transitions as photons are absorbed in the irradiated area.[14] Due to the localized accumulated energy density, particles are then removed from the bulk material in the form of vapor and eventually become ionized from the continued absorption of laser energy. This results to the formation of a dense plasma containing a wide spectrum of ion charge states including highly charged species. After the irradiation of the laser pulse, the dense plasma expands adiabatically following the pressure gradients along a direction perpendicular to the solid surface. This form of particle flux production through the intense irradiation of solid surfaces is called laser ablation. The conventional configuration of laser ablation is shown in Figure 2.1 where the laser is directed onto a flat surface to create the cloud of plasma.

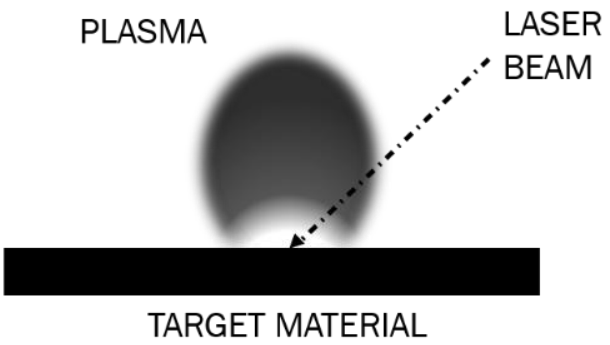

Figure 2.1. The basic configuration of laser ablation.

Since the plasma formed through laser irradiation relies mostly on the laser parameters such as energy density, pulse width and wavelength, it has been known to produce ions and neutrals based on the material composition of the laser target surface.[15] This shows the versatility in ion selection as it can be achieved by easily switching target materials to produce the required ion species for various applications. The straightforward approach to manipulate the plasma parameters is possible by adjusting the laser power density and the environmental conditions such as the addition of background gas, external magnetic fields or other parametric constraints.

The interaction of the laser to a solid surface can be divided into two scenarios, when laser energies are below and exceed the ignition threshold.[16] For the first case, the subject is focused on the thermal process where the energy is absorbed by the solid matter and results to heating the surface up to the melting point and transitions over to the next phase until it is vaporized. This process occurs extremely fast with the surface temperature rapidly increasing, close to the critical temperature, which often results to material ejection and formation of nanoparticles.[17] The second scenario is when the energy exceeds the ignition threshold where the vaporized atoms continue to absorb photons leading to the excitation and ionization of particles. The photons are

primarily absorbed through inverse bremsstrahlung and the free electrons in the light wave are accelerated to cause collision with ions and neutrals. After the first and second stage of the laser ablation process, a dense plasma is formed and it expands away from the surface. A more detailed explanation of the different stages will be discussed in sec. 2.3 under plasma expansion dynamics.

The interaction between the laser and the solid target can be described as a thermal process where the atoms absorb the energy from the photons to undergo a phase transition to gas particles. The absorption of the laser power in a material can be described by the Beer-Lambert law,

$$I(z) = I_0 e^{-\alpha z}$$

where z is the depth, α is the absorption coefficient and I_0 is the intensity on the surface after the reflection loss. Depending on the material properties, the intensity absorbed exponentially decays with depth and the reflectivity of the surface. It also shows that the magnitude of the gradient of the intensity absorbed gives a volumetric energy $\alpha I_0 e^{-\alpha z}$ equivalent to the ablated material.

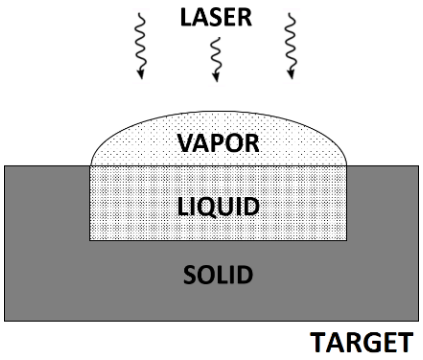

Figure 2.2. Phase transitions in laser ablation.

There are many factors on the material characteristics that influences the heat flow to the surface atoms such as the critical temperature, reflectivity, thermal

conductivity and other thermal properties. A diagram on the phase transitions during laser-induced heating is shown in Figure 2.2.

The vaporized material interacting with the photons can lead to the ionization and the formation of a dense plasma. The plasma density during the ionization process can also affect the degree of ionization of the initial dense plasma. For optically thin ionized vapor, the photons from the laser can pass through and induce the further vaporization of the surface which eventually is ionized as well. For dense plasmas on the surface, a shielding effect can occur where the laser is prevented from passing through to strike the surface and vaporize more material.

2.3 Plasma Expansion Dynamics

The dense plasma formed through intense laser irradiation adiabatically expands to free space after building up the local pressure. Due to the pressure gradients on a thin layer of dense plasma, the plasma expands to free space and preferentially perpendicular from the target surface. [18-19] This expansion of charged particles can be described in the illustration in Figure 2.3 which is dictated by the mobility of the particles and the density within the region.

The expansion of the plasma is divided into several sections starting from the bulk material and the dense plasma formed on top and eventually expanding adiabatically to free space. At the expanding region of the plasma, the fast electrons are ejected to space from the target surface followed by the ions. Since the components of the plasma are mainly electrons, ions and neutrals, they will expand accordingly based on their kinetic energies with the light and mobile electrons first followed by the massive ions. These phases in the expansion process can cause a charge separation between the

electrons and ions. This separation induces an electrostatic field that so that the electrons accelerates the ions contributing to the self-extracting nature of the plasma.

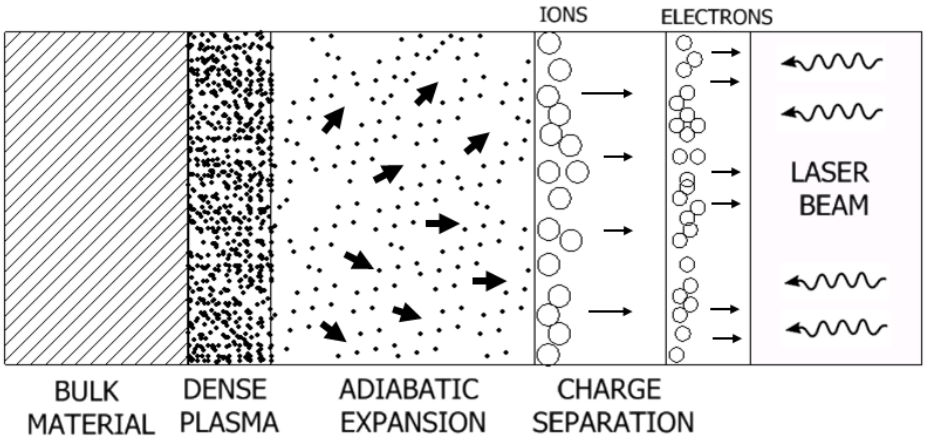

Figure 2.3. Different regimes of the plasma expansion process.

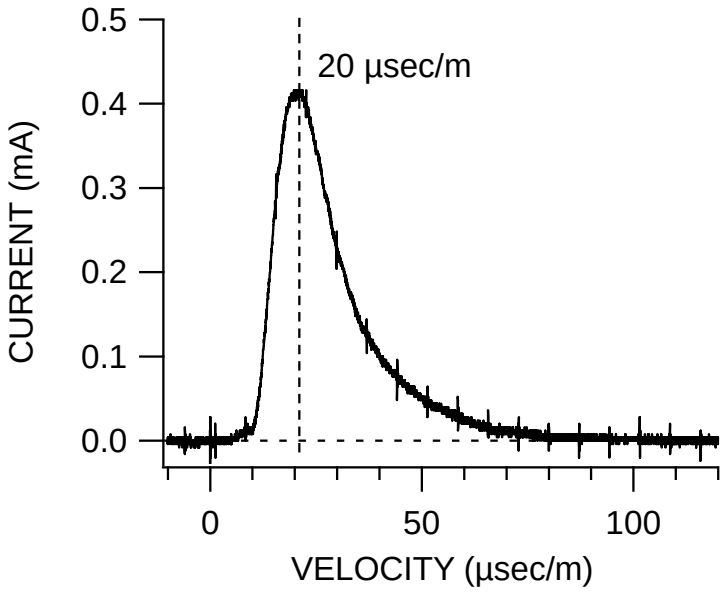

Figure 2.4 An example of a current profile of the laser produced plasma using an aluminum planar target.

Consider a planar laser target, a typical ion current signal is the distribution shown in Figure 2.4. The time-of-flight spectral data of the laser produced plasma can give information about its plasma characteristics. The shape of the distribution demonstrates the arrival of highly charged ions with the less energetic ions on the tail end of the signal. Estimating the density and the temperature of the plasma is possible through the time-of-flight profile of the ion current and the signal rise time from the plasma ignition. From the moment the laser strikes the surface, the amount of time needed to form the plasma and propagate toward the ion collector will reflect the average energy, or effective temperature of the plasma. For plasmas with the same ion species and high plasma temperatures, the signal rise time will be very short especially when increasing the laser power densities.

There are many ways to affect the size and shape of the plasma cloud during expansion. The propagation of ions can be blocked by different kinds of obstacles which can affect its free expansion. Background gases may result in the formation of shock waves in the ambient gas and cause collisional effects to the ions. Other constraints may be spatial obstruction as the ions from the plasma can cause sputtering, implantion, or adhesion to the surface or even redirect the trajectory by particle reflection.

2.4 Aluminum Planar Target Laser Ion Source

To understand the plasma dynamics in a conventional laser ion source, an experiment using an aluminum planar target was operated under a low laser power regime. A photo of the aluminum plate used as the laser target with observable surface erosion caused by laser ablation is shown in Figure 2.5. To manipulate the power density on the surface, the laser spot size and the laser power can be altered to the

desired laser irradiation conditions through the use of a condenser lens and also adjusting the q-switch delay of the laser. Since the experiments were conducted in the low laser energy regime, the irradiated area was held at the same location for each laser power density. Although the energy was sufficiently low to retain the plasma characteristics in every laser shot, the Faraday cup signal waveform was constantly monitored for signal reproducibility. More details on the experiment and analysis are found in section 6.4 of chapter 6 and the discussion here will focus on the conventional operation of a laser ion source using a planar laser target.

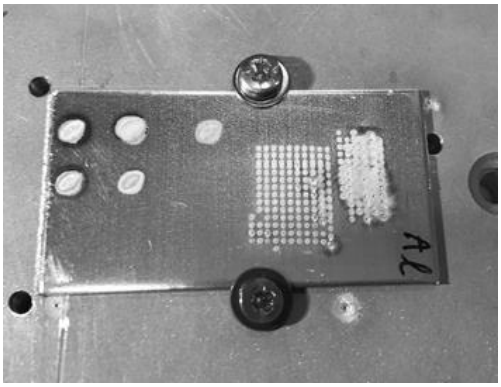

Figure 2.5 Aluminum planar target used for laser ablation.

Faraday cup measurements were taken for the laser power densities from 2.0 to 4.3×10^8 W/cm^2 and the ion currents are shown in Figure 2.6. Observing the signal profiles, the intensity increased proportionally for more intense laser power densities. The pulse width also shows the similar relation to the laser power with longer signal durations of up to 200 μsecs. Examining the onset of the signal, the rise time varies for different laser conditions with longer signal rise times for less intense laser power. A time difference of 30 μsecs is observed from 2.0×10^8 and 4.3×10^8 W/cm^2. This signal rise time gives characteristics of the plasma parameters and is an indication for the

plasma temperature as seen in the current profiles. The sharp rise of the current signals correspond to the high charge state ions generated in the plasma and the decay of the signal is determined by the less energetic ions including singly charged ions that mostly makes up the tail end of the current signal.

The measurements for the Faraday cup signal and the 90° electrostatic ion analyzer are both along the drift axis. With the retractable mechnism of the Faraday cup to the clear the path for the ion analyzer, the laser produced plasma is mass separated by bending the ion trajectory 90° using cylindrical electrodes for electrostatic deflection. The ion species are identified as aluminum ions of up to +3 charge states and other ions of oxygen, carbon and hydrogen.

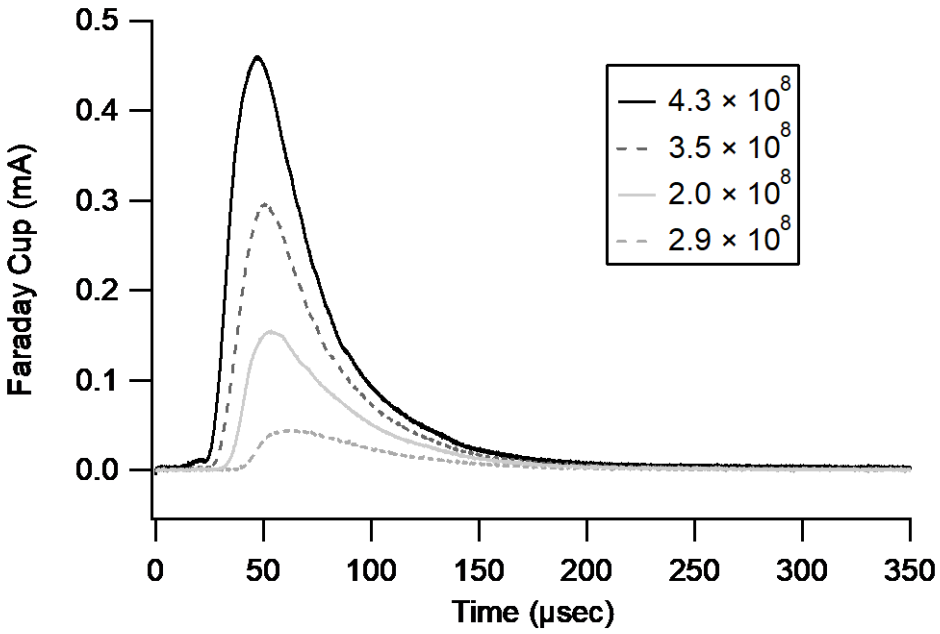

Figure 2.6 Faraday cup measurement of the laser produced aluminum plasma using different laser power densities (W/cm^2).

Since the mass separated signals gives the energy of the ion species, the analysis of the fractions of the ions in a single plasma pulse is recreated from the previously

obtained ion current signals and this allowed the estimation of the ion composition. Understanding the relation between the ion current and the drift distance of the laser produced plasma makes it is possible to analyze the measurements from different drift locations through the assumption of propagation from a point source. After adjusting the measurements accordingly, the ion current from the Faraday cup and the total number of ions were calculated to give a percentage of the ion species that make up a single plasma pulse. The number of ions as fractions of the ion species using laser power densities of 2.0 to 4.3×10^8 W/cm^2 are shown in Figure 2.7. The composition of the plasma pulse using the lowest laser power density condition was found to be highly abundant in singly charged aluminum ions with the other charge states kept below 20%. As the laser power density was increased to 4.3×10^8 W/cm^2, the amount of high energy ions grew and eventually the energies became sufficient to ionize other atoms on the target material as observed in the mass analysis.

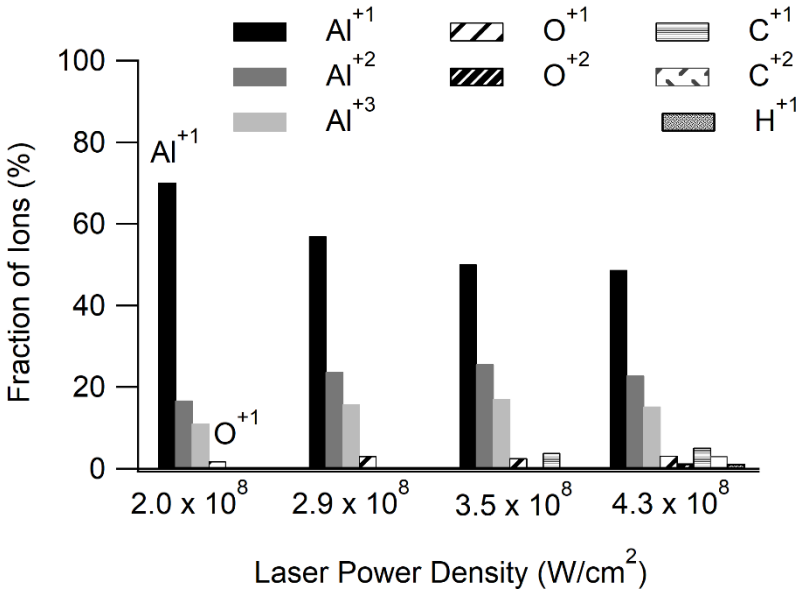

Figure 2.7 The fraction of ion species in a single plasma pulse for the different laser power density conditions.

2.5 Summary

The physics behind laser produced plasmas such as laser ablation, plasma expansion dynamics and the plasma characteristics of an aluminum plasma from a planar target are discussed. The formation of plasma through laser irradiation occurs as surface heating close to critical temperatures results to material vaporization and eventually the ionization by the incident photons. The plasma expansion after the termination of the laser pulse has different regimes where the highly mobile electrons drift outward first followed by the ions, and the charge separation induces an accelerating field that self-extracts the plasma plume toward the downstream region. The characteristics of a laser produced plasma using a planar aluminum laser target is demostrated to be used as a reference during the development and testing of a new laser ion source system.

Chapter 3

Prototype Design for the Hollow Target Laser Ion Source

"It is a capital mistake to theorize in advance of the facts. Insensibly one begins to twist facts to suit theories, instead of theories to suit facts."

-Sherlock Holmes

3.1 Introduction

Laser ion sources have drawn attention for their capability of producing a wide spectrum of charged state ions from a simple configuration. Intense pulsed laser beams in the order of 10^8 W/cm^2 consists of neutrals and positively charged ions.[20] Given the potential applications as ion sources, the self-extraction nature of the multiply charged ions often widens the energy distribution function.[21-22] Lowering the laser power density will lead to lower ion charge states but the signal intensity will be compromised. Instead, another possibility to achieve narrow energy distribution function is considered to produce a low temperature plasma through enhancing recombination. To test this possibility, the design of the ion source has been modified with the objective to generate singly charged ions and also negative ions.

The laser produced plasma initially starts with a high density state containing a wide distribution of ion charge states then expands perpendicularly to the surface due to its self-extracting nature. With the decrease in the density as the ions move toward the low-pressure region, the rate of recombination also decreases and this allows the ions to retain the charge state distribution for longer periods. During this expansion phase of the plasma, an addition of geometrical constriction can affect the expansion of the ions. For instance, the addition of magnetic fields extends the pulse duration of the plasma. Geometrical constriction, however, introduce additional collision mechanisms and possibly dissipate the kinetic energy of the particles. Since cooling down of the plasma will lead to lower ion and electron energies, this will increase the probability of molecules, clusters and also negative ion formation. To understand the fundamental properties of spatially confining an expanding plasma, the geometry of the target was designed to have a hollow cylindrical shape with the plasma ignited inside the conduit.

In this chapter, initial experiments using the prototype design for a laser ion source is investigated. Observations through high speed images and time-of-flight measurements were conducted to test the ion production using the unique laser target. Fundamental atomic-molecular processes are also introduced to the expanding plasma. By injecting neutral gas to the plasma region, the collision rate within the plasma is increased to cool down the plasma and increase the probability of producing negative ions by dissociative attachment. The operation of the hollow cylinder target laser ion source is assessed for the possibility of singly charged positive and negative ion production.

3.2 Hollow Cylinder Target

The dependence of the plasma parameters to irradiation conditions such as the laser energy, wavelength and target material has been immensely studied to control the laser produced plasma. To tune the laser ion source to the desired range of charge state ions, the laser parameters are adjusted, specifically the laser energy, keeping it to the level necessary to generate the ion with the particular charge state. Aside from controlling the plasma through the laser parameters, allowing the highly-charged ions to interact with atoms can effectively cool down the plasma through atomic collisions. This concept can be applied to a laser produced plasma through spatial confinement during the expansion phase.

The prototype laser target which is made from amorphous graphite is designed with a hollow cylindrical shape to cause a geometric constriction to the laser produced plasma. As the laser beam is guided to a narrow volume generating plasma in the confined region, the hollow structure allows the buildup of pressure and induce collisional effects that can lower the bulk electron temperature of the plasma. The design of a conduit type target will also allow the oblique extraction of ions with the plasma plume flowing out of the structure during expansion. Centered along the axis of the system by an aluminum enclosure, the graphite target is fixed securely as shown in Figure 3.1. The target has a hollow cylindrical structure with 10 mm inner diameter and a total length of 30 mm. The backside of the graphite target has an 8 mm opening to allow the laser beam to strike the surface at an angle of 30° from the target axis.

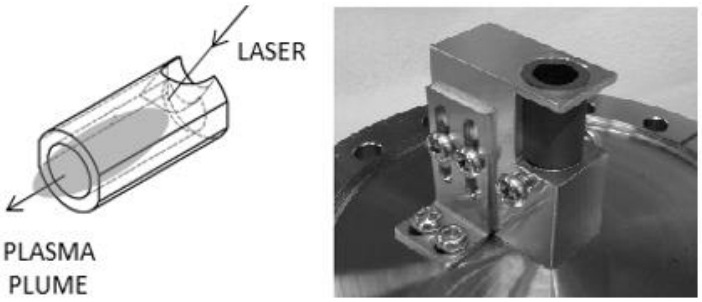

Figure 3.1 Design of the hollow cylinder target assembly.

3.3 Experimental Setup

Using a Q-switched Nd:YAG laser operated at 1064 nm, the beam is focused to a spot size of 1 mm by a condenser lens on the target surface to produce plasma inside the 10 mm diameter volume. A schematic diagram of the experimental setup is shown in Figure 3.2. Inside a 95 mm diameter, 200 mm cylindrical stainless steel chamber, the graphite target is mounted at the center of the axis with a Faraday cup assembly installed at the other end of the chamber 270 mm away from the target. Dipole magnetic configuration using two Neodymium magnets with 100 Gauss at the axis of the Faraday cup was attached 40 mm from the opening of the collector to exclude electrons coming into the cup.

On the front side of the target, a nozzle aiming at the opening injects helium gas into the expanding plasma region. The introduction of neutral gas to the system induces collisional effects to increase the probability of recombination and dissociative electron attachment for less energetic ions and negative ion production. Experiments are conducted using a time-of-flight analyzer coupled to a Faraday cup system and a 12,300 fps high speed camera with the trigger synchronized to the Nd:YAG laser Q-switch.

The pulsed Nd:YAG laser system, having a maximum average pulse energy of 2 J at a 10 Hz repetition rate, was operated at lower laser power density conditions by adjusting the Q-switch delay of the system. Power measurements were made through a photodetector with the laser intensity reduced to a factor of 200 and was correlated to the Q-switch delay settings. To avoid breaking the target, the delay is adjusted at a certain range so that the laser power is controlled at a linear rate.

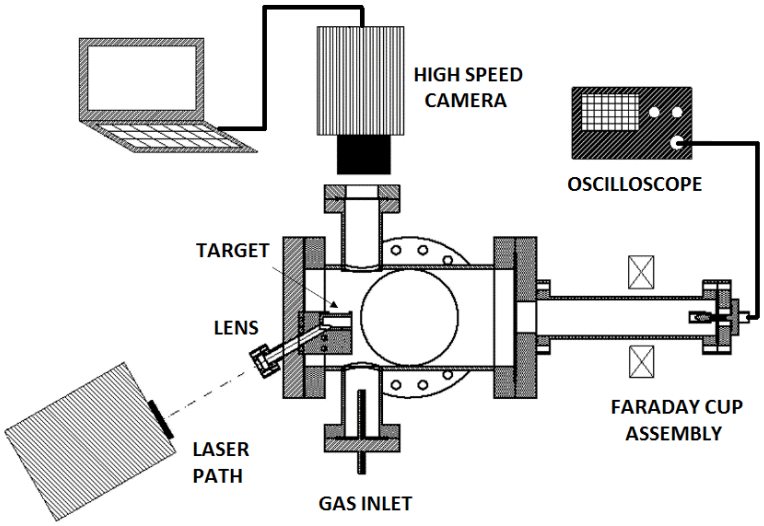

Figure 3.2 Schematic diagram of the laser ion source.

Table 3-1 Operational parameters for the Laser Induced Plasma.

Laser power density	9.0 – 16.0 GW/cm^2
Pulsewidth	5 nsec
Wavelength	1064 nm
Target material	Graphite
Angle of Incidence	30° (from the axis)
Base Pressure	1.0 x 10^{-5} Pa
Gas Species	Helium

3.4 Results

The initial experiments performed using the prototype laser ion source system are discussed in this section. The visual observations of the laser produced plasma through high speed images and the corresponding time-of-flight signals from the Faraday cup are analyzed to study the dynamics of the plasma formed using a hollow cylindrical target.

3.4.1 High Speed Camera Image

High speed images with a front view of the target were captured as the laser was directed to the surface of the graphite target. The images in Figure 3.3. of the laser ablation process by looking into the graphite tube shows the rapid expansion of the a luminous cloud perpendicular to the material surface after the initial thin glow.

At higher laser power density greater than 13.5 GW/cm^2, the glowing region occupies the entire volume of the tube. Immediately after the expansion, the cloud is extinguished in the surrounding space leaving a thin silhouette of an afterglow. The observable duration of the luminous cloud formation and expansion lasts for 405 μsec for laser power density 13.5 GW/cm^2. Small light emitting dust are observed in the plasma as the laser power density exceeded 1.50 GW/cm^2 indicating that mass removal occurs on the target surface.

To further investigate the flow of the cloud out of the conduit, images from the side of the target were obtained as shown in Figure 3.4. Due to the extremely fast expansion of a laser produced plasma, typically occurring within several microseconds, only one image was obtained with a side perspective at the target exit. The side view image also corresponds to the maximum brightness of the expanding cloud inside of the hollow

target since the bright glow will only extend out after the pressure builds up inside. This suggests that the duration of the luminous cloud reaching outside the target is less than several microseconds.

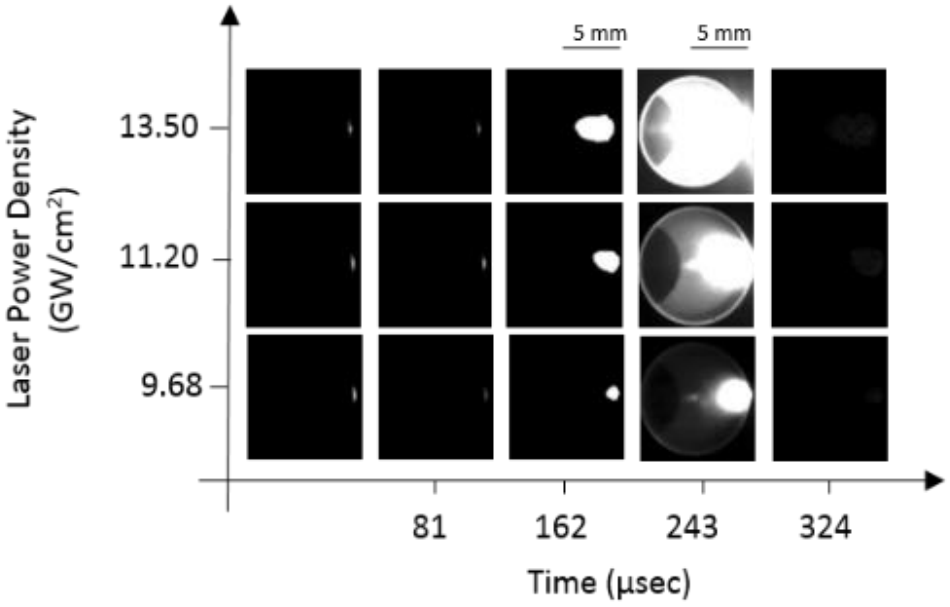

Figure 3.3 Image sequence of a luminous cloud inside the graphite target in vacuum for the laser power densities 9.68, 11.2 and 13.50 GW/cm^2.

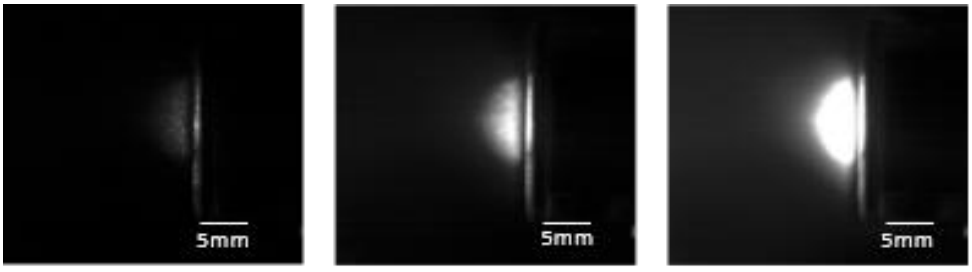

Figure 3.4 Images of a radiant glow flowing out of the hollow cylinder graphite target with laser power densities (a) 9.68 (b) 13.50 and (c) 17.30 GW/cm^2.

The side perspective of the bright cloud extending out of the hollow target shows the concentration of the light at the exit of the cylinder. As the laser power density was increased up to 17.3 GW/cm^2, the light becomes more intense with a plume shape. The length of the plume was calculated by measuring the intensity profile with the threshold one fifth of the saturation value along axis of the hollow cylinder. The average distance from the target opening as a function of the laser power density is shown in Fig. 5 and the average length extended up to 9.16 mm at 17.3 GW/cm^2.

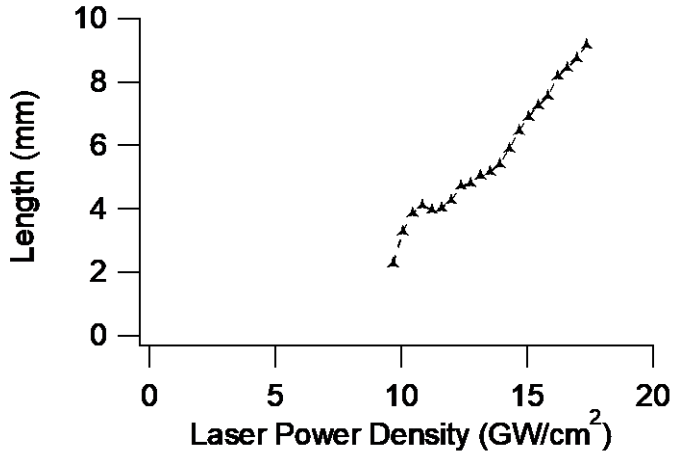

Figure 3.5 Average plume length as a function of the laser power.

3.4.2 Faraday Cup Measurements

The time-of-flight spectrum was measured for the laser induced plasma in vacuum with a base pressure of 1.0 x 10^{-5} Pa shown in Fig. 3.6. The signal duration of the plasma pulse was observed to be less than 1 μsec and signal shows a negative peak of -51 mA at the beginning of the plasma pulse indicating a burst of electrons from the outer layer of the plasma. Afterwards, the current detected by the Faraday cup shows the decay of the ion current that follow for a time interval of 0.9 μsecs. As laser power density was

increased above 14.3 GW/cm^2, the ion current duration broadened and the formation of two peaks was observed at 95 and 200 nsec from the onset of the signal.

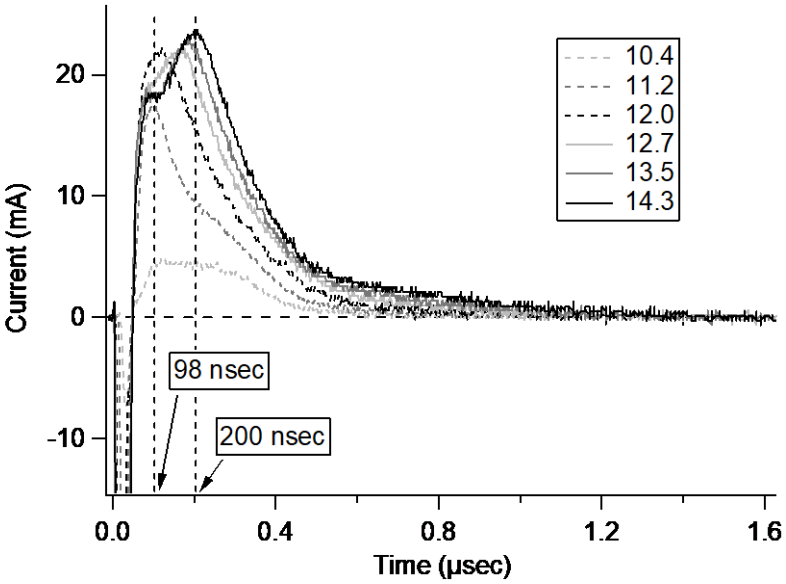

Figure 3.6 Time of flight measurements for the laser produced plasmas at varying laser power densities (GW/cm^2) with a base pressure of 1.0 x 10^{-5} Pa.

To increase the probability of reducing the density of highly positive ion charges and producing negative ions, neutral gas is injected to the plasma region to increase the collision frequency and to reduce the bulk electron temperature. Time-of-flight measurements were taken at a helium gas pressure of 2.0 x 10^{-1} Pa at laser power density of 13.5, 14.3 and 15.0 GW/cm^2 the measured signals are shown in Fig. 3.7. A positive signal that lasted up to 44 μsecs was observed before the negative signal corresponding to negative ions were detected. The time duration of negative ions is about 500 μsec which is significantly longer compared to the positive ions. At a laser power of 15.0 GW/cm^2, the signal reached a maximum of -80 mA.

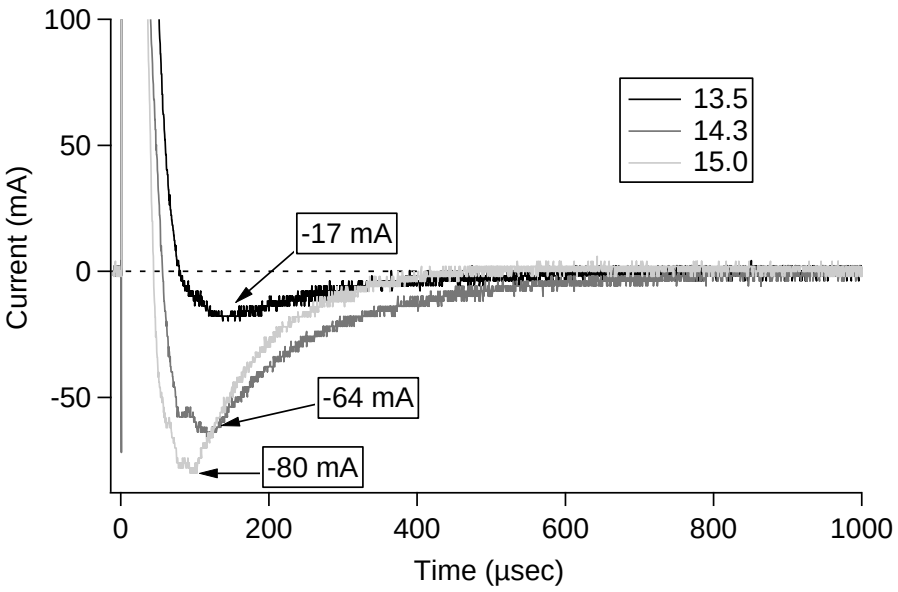

Figure 3.7 Time of flight measurements for laser produced plasmas at varying laser power densities (GW/cm^2) with a background helium gas pressure of 2.0 x 10^{-1} Pa.

3.5 Discussion

The laser ablation process observed from the high-speed images showed the sequence of plasma formation from a thin strip of light to a bright cloud expanding inside the hollow cylinder. As the laser power density was increased, the luminous cloud grew in size and occupied the volume of the target. With the laser energy absorbed by the target surface, light emitting dust have also been detected signifying a surface phase explosion due to the intense laser irradiation. The mass removal was observed clearly when operating with higher laser power densities. This phenomenon is detrimental to a continuous system operation since the lifetime of the target will be reduced due to the localized surface deterioration.

Obtaining both the front and side image perspective of the target, the progression of the observed cloud formation and expansion process is examined for the effects of

geometric constriction. Observations show the observed glow undergoes an expansion process inside the hollow cylinder which lasts for about 400 μsec but only flows out of the target with a shorter duration estimated to be less than 80 μsec. During the expansion phase, the bright cloud strikes the inner wall of the target and is constrained inside the cylindrical volume. The buildup of pressure eventually effuses the observed luminous vapor to the downstream region. In relation to the Faraday cup signal measurements, the charged particles that leave the hollow target are measured with the signal duration to be very short occurring within 1 μsec. This explains that the ion formation from the laser produced plasma is occuring faster than the luminous cloud observed in the images. One possibility for the bright glow from the images are vapor coming from the afterglow of the plasma formation as the duration was longer than the actual ion signals measured from the Faraday cup. The laser flash lamp duration also occurs around several hundreds of microseconds and the possibility of light leaking through and focusing on the surface can cause the formation of a bright cloud seen in the images. Further investigation should be conducted to the observe the actual plasma formation and expansion inside the cylindrical target.

After the dense plasma formation, along with the termination of the laser pulse, charged particles expand adiabatically from its initial dense state with the highly mobile electrons first and then followed by ions. From the Faraday cup measurements, a negative peak of the energetic electrons in the onset of the signal has confirmed the charge separation between the ions that fall behind the electron ejection which contributes to the ion acceleration by electrostatic forces. By increasing the laser power, the measured ion current was amplified and the formation of two peaks were detected at a laser power density of above 12.7 GW/cm^2. The characteristic in the signal suggests a possibility of a secondary laser ablation process inside the target volume due to multi-

photon plasma reflection at higher laser power densities. With the laser beam redirected to another surface, the formation of a new dense plasma region causes the prolonged ion emission signal. The constrained plasma expansion within the volume of the target can also induce plasma by ion-atom collisions on the area adjacent to the initial laser produced plasma. This additional source of ions can contribute to the increase in the ion signal of the second peak. The possibility of space beam loss caused by the space charge after ion and electron separation are also considered. Neutrals and ions with lower energies produced in the plasma cloud can also undergo ionization by subsequent collisions with highly charged ions and this can also be a factor in the time interval found in ion signal. Utilizing a hollow cylindrical target structure a mechanism has been observed to introduce an additional process that prolongs the duration of the laser produced plasma signal.

Introducing background neutral gas in the downstream region of the system allows the injected gas to interact with the plasma particles that leave the hollow target to achieve a reduction in the bulk electron temperature and increase the probability of producing negative ions. To test the possibility of negative ions production, a Faraday cup with a dipole magnetic filter for electron suppression measured signals from the laser produced plasma with background neutral gas. The measured ion current detected negative signals that correspond to negative ions that arriving at a later time after the positive ion peak. The positive signals from the Faraday cup measurements without background neutral gas only has a duration of around 1 μsec as compared to the 44 μsec duration observed in the Faraday cup measurements with background neutral gas. Although the measured signals had a large disparity in signal durations with the addition of background neutral gas, this explains an increase in the signal intensity along with its duration for conditions with helium gas in the expansion region.

Increasing the laser power density also enhanced the negative ion signal and the addition of background neutral gas to the laser produced plasma is a promising method to generate negative ions.

3.6 Conclusion

A laser ion source is being developed for the production of positive and negative singly charged ions. The design of a hollow cylinder target is employed to constrain the laser induced plasma inside a small volume of a hollow cylinder target. Using a high speed camera, observations were made to observe the process inside the target and out of the target opening. The time-of-flight spectrum was measured to study the different phases of the laser produced plasma. The formation of two peaks was observed for laser ablation in vacuum using higher laser power densities. With the addition of background neutral gas, time-of-flight measurements were obtained and a signal corresponding to negative ions was detected 44 μsec from the start of the plasma signal with a maximum of 80 mA at a laser power density of 15.0 GW/cm^2. The duration of the signal was significantly longer compared to that of the positive ions. The initial experiments on the prototype laser ion source demonstrates the laser produced plasma with geometric constriction and further analysis on the plasma parameters will evaluate the performance of the system.

Chapter 4

Plasma Diagnostics of the Laser Produced Plasma

"It doesn't matter how beautiful your theory is, it doesn't matter how smart you are. If it doesn't agree with experiment, it's wrong."

-Richard Phillips Feynman

4.1 Introduction

High intensity laser beam directed on a solid surface forms a dense plasma that expands perpendicularly to the surface. The wide spectrum of charge state ions including highly charged species formed through the use of a simple configuration has drawn attention to its application to fields such as materials science and ion beam physics. Solid materials such as graphite and aluminum can serve as sources to generate nanoparticles and functional thin films by pulsed lasers which have significant roles in electronic applications.[23-24]

When the laser reaches a solid surface, the formation of the plasma can be represented by a series of different stages of plasma-material interaction in a short time-frame. The early stages of the plasma formation involve the absorption of photons into the solid surface and accumulation of local energy density which leads to the ejection of electrons and atoms. The second stage is the formation of a highly dense plasma as ejected atoms from the surface continue to absorb energy from the laser

irradiation until it becomes ionized. During this stage, the plasma is extremely dense with a high electron energies as multiple charged ions are present in the plasma. Lastly, upon the termination of the laser pulse the dense plasma expands to the surrounding space and the thermalization of energetic electrons realizing the condition to characterize the electron temperature of the produced laser plasma. Understanding the dynamics in the final stage of the plasma expansion is important since the cooling down of the plasma will lead to lower ion and electron energies and formation of molecules, even clusters.

The interaction of the laser and the plasma plays an important role during the plasma expansion in the laser ablation process. Altering the target geometry will introduce additional collision processes by spatially confining the expanding plasma. To apply this concept, a hollow-cylinder laser target has been utilized to produce plasma by directing a laser beam to strike the inner walls of the narrow conduit. Initial experiments of the prototype system have observed the rapid expansion of the plasma constrained by the target geometry. As the plasma expanded from the surface, it eventually occupied the entire volume of the hollow target before flowing out of the cylinder. Utilizing such a structure has affected the adiabatic expansion of the laser produced plasma by allowing it to interact to the surface atoms. This increases the possibility of sputtering or ionization of neutrals and ions near the surface so that the kinetic energies can be further dissipated and effectively lower the plasma temperature. To evaluate the plasma properties, an investigation on the plasma parameters and the propagation of the laser produced plasma will be discussed in this chapter.

Plasma diagnostics are conducted to examine the optical emission characteristics, probe signal measurements including Langmuir probe analysis of the laser produced plasma. High electron temperatures in plasmas will only increase the probability of

electron detachment which is detrimental to negative ions production. Thus, confirming the effectiveness of the laser ion source in achieving a low electron temperature condition which is essential for realizing the conditions for negative ion formation.

4.2 Plasma Diagnostics

Studying the characteristics of the laser produced plasma requires a background on some basic concepts of physics to analyze the information obtained from the plasma diagnostic experiments. A brief review of spectral line emission and radiance, current-voltage characteristics of plasmas will be covered in this section.

4.2.1 Plasma Spectroscopy

When a photon interacts with a particle, the energy can be absorbed to excite the atom, moving the state to a higher quantum level. As the atom reverts back to a lower state, spontaneous emission occurs emitting a photon with a characteristic energy of the transition of the two states.[25]

$$\mathbf{E} = \hbar\omega = E_2 - E_1$$

This radiative decay is reflected as a spectral line in the electromagnetic spectrum and is often used to identify atoms and molecules. An example of an optical emission spectra is shown in Figure 4.1 with strong emission lines that correspond to mercury ions from a gas-discharge lamp.

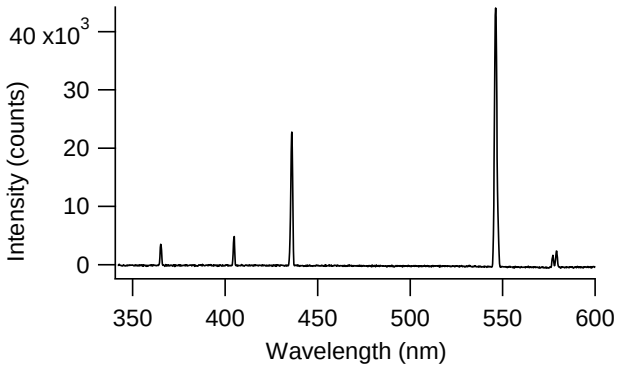

Figure 4.1 Line emission of argon ions.

For electromagnetic radiation in thermal equilibrium conditions, radiation emission occurs and the spectrum of thermal energy is described by the Planck distribution function or the thermal average number of photons in a single mode frequency given by,

$$\langle s \rangle = \frac{1}{\exp\left(\hbar\omega/_{T}\right) - 1}$$

where T is the temperature and ω is the frequency. This describes the spectrum of electromagnetic radiation in thermal equilibrium in a cavity.[26] From the Planck distribution, the thermal average energy can be written as $\langle \varepsilon \rangle = \langle s \rangle \hbar\omega$ where the radiation is regarded as photons. Then the total energy of the photons in the cavity would then be the summation of the energies for the all the modes, $U = \sum_n \langle \varepsilon_n \rangle$. Integrating the total energy over a volume V will give the energy per unit volume and will yield,

$$\frac{U}{V} = \frac{\pi^2}{15\hbar^3 c^3} T^4$$

which is also known as the Stefan-Boltzmann law of radiation where the radiant energy is proportional to the fourth power of the temperature. From this law, the radiant

energy of a volume per frequency can be derived which is known as the spectral density. The equation is given by,

$$u_\omega = \frac{\hbar}{\pi^2 c^3} \frac{\omega^3}{\exp\left(\hbar\omega/_T\right) - 1}.$$

This spectral radiance as a function of frequency gives the distribution of thermal radiation. The temperature of the black body can be found at the frequency where the radiance is at maximum.

4.2.2 Electrostatic Probe Theory

The current-voltage characteristics of the plasma provides many information about the ions, electrons and other important plasma parameters. By inserting a collector probe to the plasma region and scanning the bias voltage from a negative to positive potential, the measurement of the probe current I_p will give a characteristic curve as shown in Figure 4.2. The analysis of the I-V curve will help determine the plasma parameters such as the electron density, electron temperature and the plasma potential. [27]

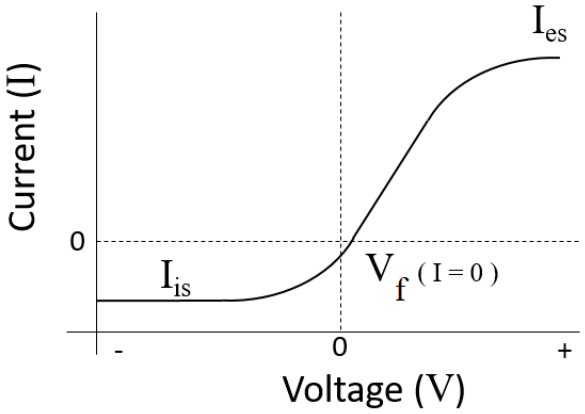

Figure 4.2 Ideal I-V characteristics of a plasma.

If the potential on the probe is negative with respect to the plasma potential, the ions are collected to give the ion saturation current, I_{is}. Equation (4.1) shows the ion current I_i as a function of the bias voltage V_b in a Maxwellian ion distribution at temperature T_i.

$$I_i(V_b) = -I_{is} \exp\left[\frac{e(V_p - V_b)}{k_B T_i}\right], \qquad V_b \geq V_p \qquad (4.1)$$

where e is the electron charge, k_B is the Boltzmann constant, T_i is comparable to the electron temperature T_e. When the bias voltage is smaller compared to the plasma potential, only ions will be collected and ion current will be reach a saturation commonly referred to as ion saturation current I_{is}. As the voltage becomes less negative, energetic electrons are then collected and ion current eventually becomes zero, $I_i = 0$. The ion saturation current I_{is} is given by,

$$I_{is} = \frac{1}{4} e n_i v_{i,th} A_{probe} \qquad (4.2)$$

where the ion thermal speed is $v_{i,th} = \sqrt{\frac{8k_B T_i}{\pi m_i}}$. The dependence to the electron temperature is related to the formation of a sheath around a negatively biased probe. If the potential of the probe is different from the plasma potential, the electrons and ions distribute spatially in order to shield its effect on the bulk plasma. A negative sheath is then formed for a positively biased probe whereas a positive sheath is formed for a negatively biased probe. Similarly, for the electron current I_e as a function of the bias voltage,

$$I_e(V_b) = I_{es} \exp\left[-\frac{e(V_p - V_b)}{k_B T_e}\right], \qquad V_b \leq V_p \qquad (4.3)$$

and the electron saturation current I_{es} is given by,

$$I_{es} = \frac{1}{4} e n_e v_{e,th} A_p \qquad (4.4)$$

where the electron thermal speed is $v_{e,th} = \sqrt{\frac{8k_BT_e}{\pi m_e}}$. Rewriting the equation for $I_e(V_B)$ using equations (4.1), (4.3) and (4.4) for $V_B \leq V_p$ will give,

$$\ln\left|I_{probe} - I_{is}\right| = \frac{e}{k_BT_e}(V_P - V_B) + \ln\left[en_eA_{probe}\sqrt{\frac{k_BT_e}{2\pi m_e}}\right] . \qquad (4.5)$$

This shows the linear dependence of $\left|I_{probe} - I_{is}\right|$ on $(V_P - V_B)$ with the slope corresponding to the electron temperature.

4.3 Experimental Setup

Diagnostic experiments are conducted in the laser ion source system to examine the properties of the laser produced plasma. Optical and electrostatic diagnostic techniques are performed in the downstream region of the chamber and the experimental setup is shown in Figure 4.3.

A high speed camera was focused using a 0.9 m lens to give a clear picture from two perspectives, the inside and outside the hollow target. The optical emission spectra of the plasma formed through laser ablation was obtained using a USB4000 Ocean Optics spectrometer with a 0.22 nm resolution to determine the ion species present in the plasma. To further investigate the trajectory of the plasma along the axis of the target, 1.5 mm diameter tungsten probes with a 0.28 cm^2 surface area and 2 mm radial offset from the center axis of the target were positioned 5 and 10 mm away from the target opening. The two probes were connected directly to an oscilloscope to measure the ion signal as the laser produced plasma expands outside of the conduit. Signals of the probes were measured by voltage induced on 1 MΩ oscilloscope inputs with 50 Ω termination resistors.

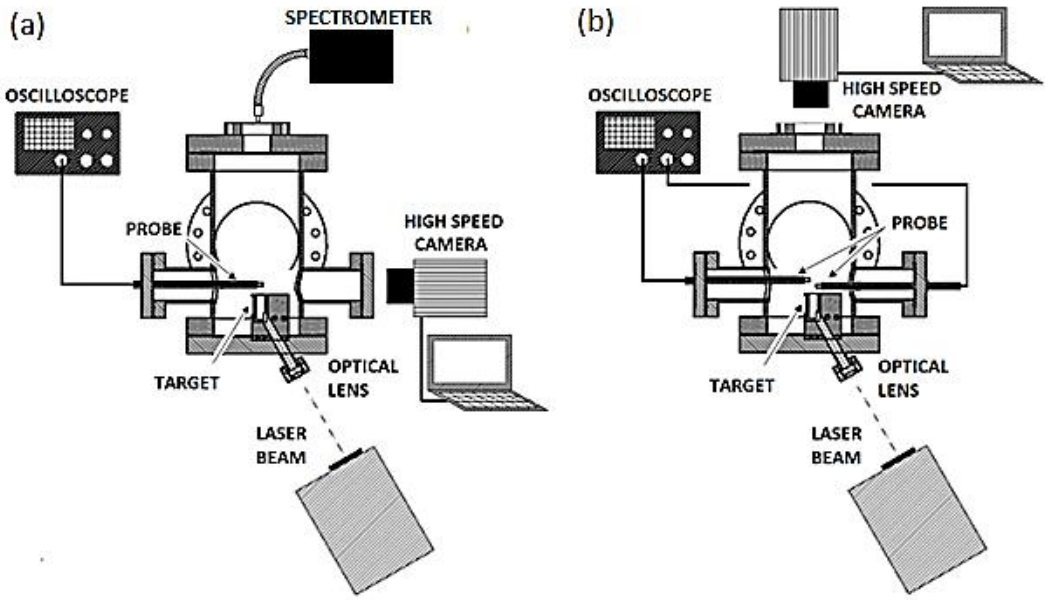

Figure 4.3 Laser ion source: Schematic diagram of the system: (a) probe current experiment, and (b) space resolved probe experiment.

For the Langmuir probe analysis, the tungsten probe was positioned on the axis at 15 mm away from the exit of the hollow target. Using a frequency generator to supply an oscillating voltage signal at 100kHz and amplified to $\pm$8V, the input and probe voltages were measured to obtain the probe current across a 1kΩ resistor. Plotting the I-V curve generated from the voltage measurements, the ion saturation current I_{is} can be observed in the negative portion of the voltage sweep. After obtaining the value of I_{is}, the $\ln |I_{probe}\text{-}I_{is}|$ is then calculated and plotted over the voltage applied to the probe to deduce the electron temperature in eV. The plasma potential is also determined from the intersection of the slope and the linear fit of the saturation region.

The hollow cylinder target material used in all the diagnostic experiments is graphite. The prototype target design was modified to have an inner diameter of 7 mm

to observe the effect of a narrower volume on the plasma expansion. Another feature was added to the cylindrical wall thickness which was increased to 6 mm on the laser irradiation side to compensate for the crater formation and extend the lifetime against continuous ablation. For the optical emission spectroscopy and high-speed images, an aluminum material for the hollow cylinder target was tested and included in the diagnostic experiments.

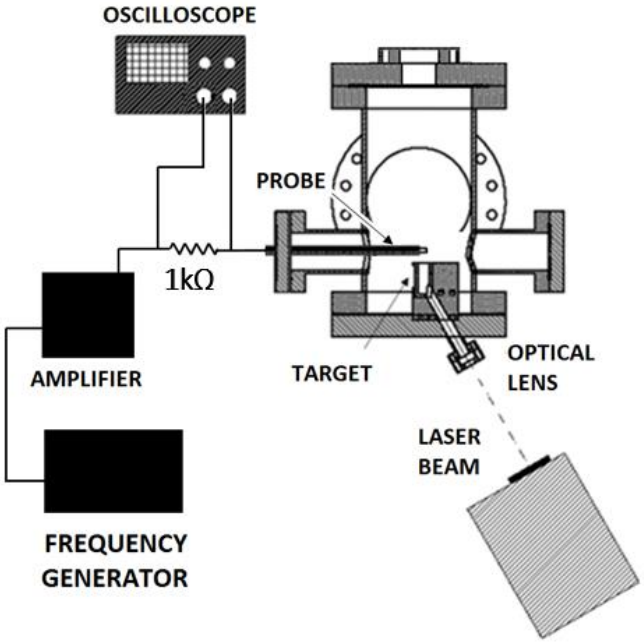

Figure 4.4 Diagram of the experimental setup using a Langmuir Probe.

4.4 Results

Initial experiments are performed for the first time with the prototype laser ion source that uses a hollow cylindrical type laser target. The characteristics of the plasma is observed through the high speed images of the laser ablation process and the time-of-flight measurements of the self-extracting ion escaping the hollow volume of the target. These experimental results will be described in more detail in this section.

4.4.1 Optical Diagnostics

Images captured using a high-speed camera showed the luminous cloud formation inside a graphite target with 7 mm inner diameter. The sequence of the laser ablation process shown in Figure 4.5(a) displayed the rapid expansion on the surface using a laser power density of 10.4 GW/cm^2 with frame intervals of 13.79 μsec. Similar to the initial experiments, the expansion occurs perpendicular to the surface and towards the adjacent area of the irradiated spot. By examining the images after the intense light of the plume more closely, a larger amount of light emitting dust moving in different directions could be observed as compared to the previous 10 mm diameter target design.

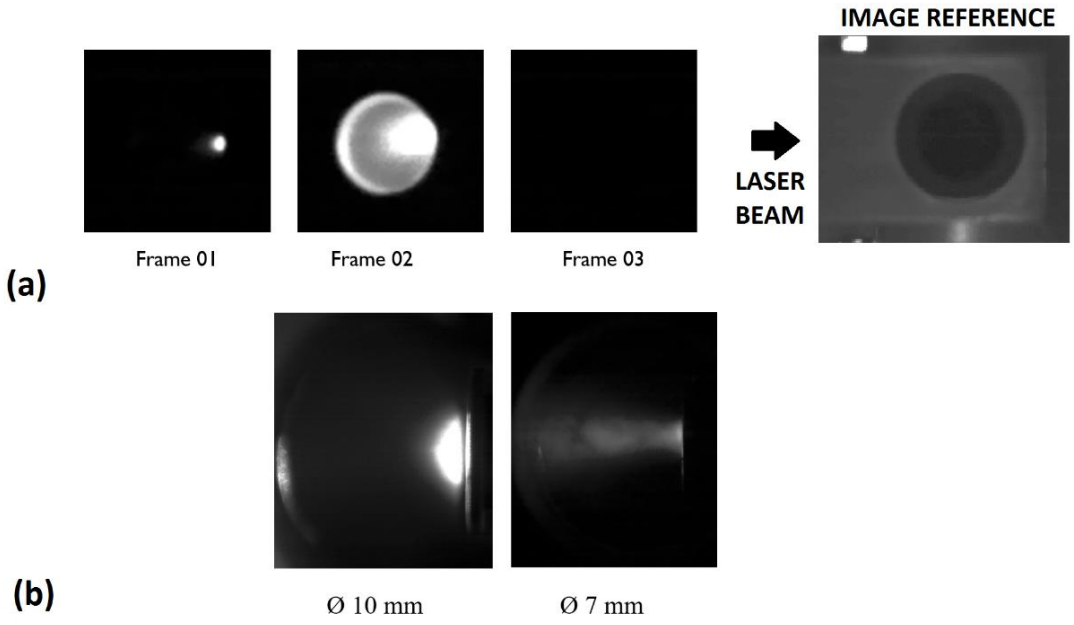

Figure 4.5 Images during the laser irradiation. a.) inside the target with 7 mm diameter, and b.) flow out of the target using inner diameter dimensions of 10 and 7mm.

The images in Figure 4.5(b) show the side view of the graphite tube and the bright plume flowing out of the target for the target dimensions with inner diameters of 10 and 7 mm. A concentrated glow was observed near the target opening for the 10 mm inner diameter, as the bright cloud expanded out of the conduit. However, the target structure with a 7 mm inner diameter had a more diffused light with less intensity but the shape of the plume appeared to be longer.

The image of the plume flowing out of the target could only be seen when the laser power density exceeded 15.0 GW/cm^2. Reducing the dimension of the inner diameter by 3 mm significantly affected the propagation of the plume as observed by the diminished light intensity in the image.

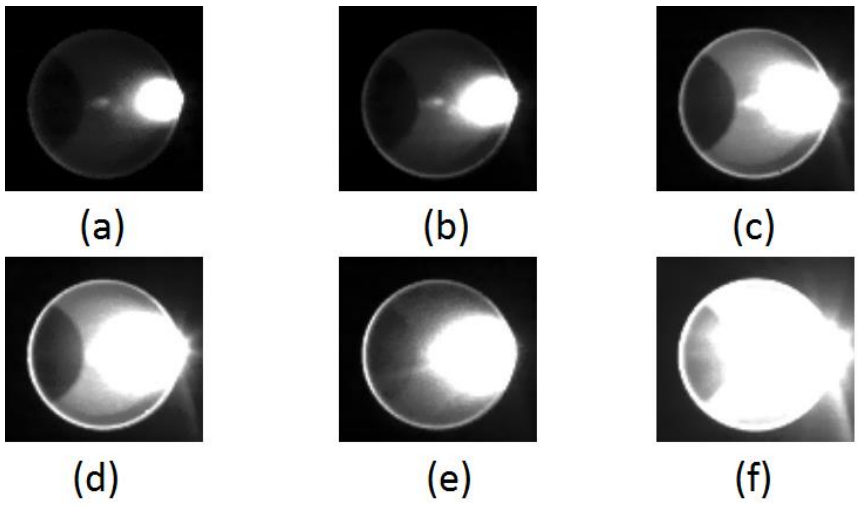

Figure 4.6 Front images of the plume inside the graphite hollow cylinder target with laser power densities of (a) 3.5, (b) 4.1, (c) 4.7, (d) 5.3, (e) 5.9, and (f) 6.5 GW/cm^2.

The laser irradiation inside the hollow cylinder target having an inner diameter of 10 mm is shown in Figure 4.6 as the laser power density was increased from 8.9 to 16.6 GW/cm^2. The images show the brightest frame for the luminous cloud expansion before

it vanishes in the succeeding frames. For the graphite target, the bright center of the cloud is clearly seen in the images with the size increasing as the laser power density was doubled. The central part of the light was estimated to be 3 mm in diameter and gradually expanded to fill the entire cylinder. Soft luminous spots are also detected in the surrounding edge of the bright cloud for the lower laser power densities.

Similarly, the glow produced from an aluminum target material was detected at laser power densities lower to the conditions for the graphite target. The images of the maximum brightness of the expansion are shown in Figure 4.7. Due to the high reflectivity of aluminum materials, the captured images for the aluminum target had the intense light reflection inside the cylinder during glow formation.

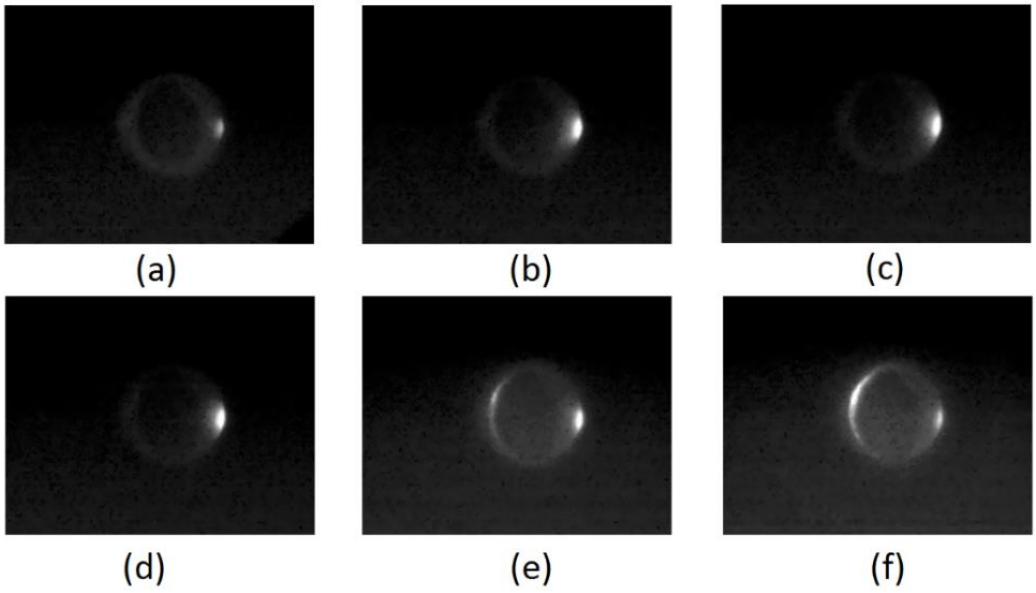

Figure 4.7 Front view Images of the aluminum hollow cylinder target with increasing laser power densities, (a) 3.5, (b) 4.1, (c) 4.7, (d) 5.3, (e) 5.9, and (f) 6.5 GW/cm^2.

Using laser power densities from 3.5 to 6.6 GW/cm^2, the small bright light was captured with rates of 33 μsec per frame, which intensified with increasing laser power densities. For the image with 5.9 GW/cm^2 laser power density, the adjacent side of the irradiated spot reveals a light reflection from the luminous cloud which becomes more distinct at a more intense laser power density.

With a clear view of the plasma expansion inside the hollow target, the optical emission spectrum was measured to determine the ions species produced in the laser produced plasma. Since the plasma expansion has a duration of only several microseconds, the measurement was integrated and a time averaged result.

Using a graphite hollow cylinder target, the emission spectra of the plasma is shown in Figure 4.8. The strong emission lines reveal singly charged carbon ions were observed with emission lines for C^0, C^{1+}, C^{2+} and C^{3+}. Using the laser power densities 13.5, 15.0 and 16.6 GW/cm^2, a background continuum in the range of 350 nm to 800 nm was detected along with the emission lines and was observed to increase with greater laser power density. Although the presence of multiple charged ions implies a high plasma temperature, the background continuum observed in the measurement suggest the plasma temperature in the order of several thousand Kelvin. As the plasma is not in equilibrium and high energy electrons, the OES data have to be interpreted as a time averaged information.

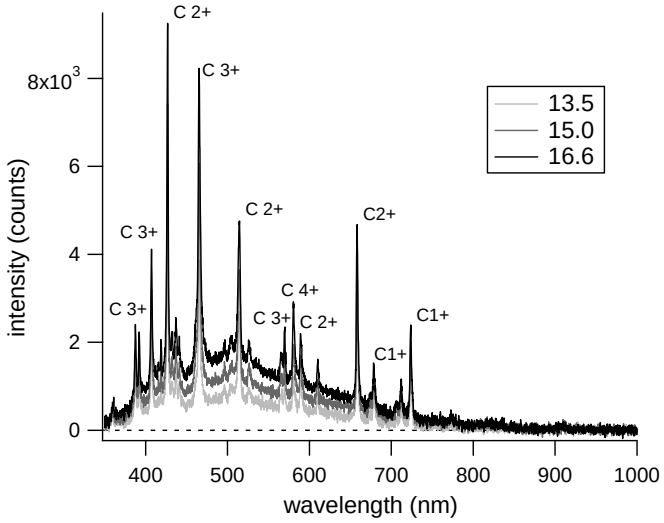

Figure 4.8 Optical emission spectra of the laser produced plasma using a graphite hollow cylinder target.

The optical emission spectrum obtained for the plasma using the aluminum hollow cylinder target is shown in Figure 4.9. Similar to the emission spectra of the carbon plasma, there is a background continuum in the broadband spectrum that indicates the thermalization of the plasma. This implies the plasma temperature to be comparable to the carbon plasma. The prominent emission lines in the spectrum were identified to be aluminum, carbon, oxygen and iron where the other elements come from the target material quality and the thin oxide layer during atmospheric exposure. Singly charged aluminum ions and neutrals were detected for the laser power densities of 4.1 to 5.3 GW/cm^2. To confirm the aluminum ion peak detected in the broadband spectra, a 0.02 nm resolution spectrometer in the range of 350 to 480 was used to measure the spectrum. Examining the emission lines, the doublet state aluminum ions could be distinguished from the peaks located at wavelengths 394.42 and 396.15 nm.

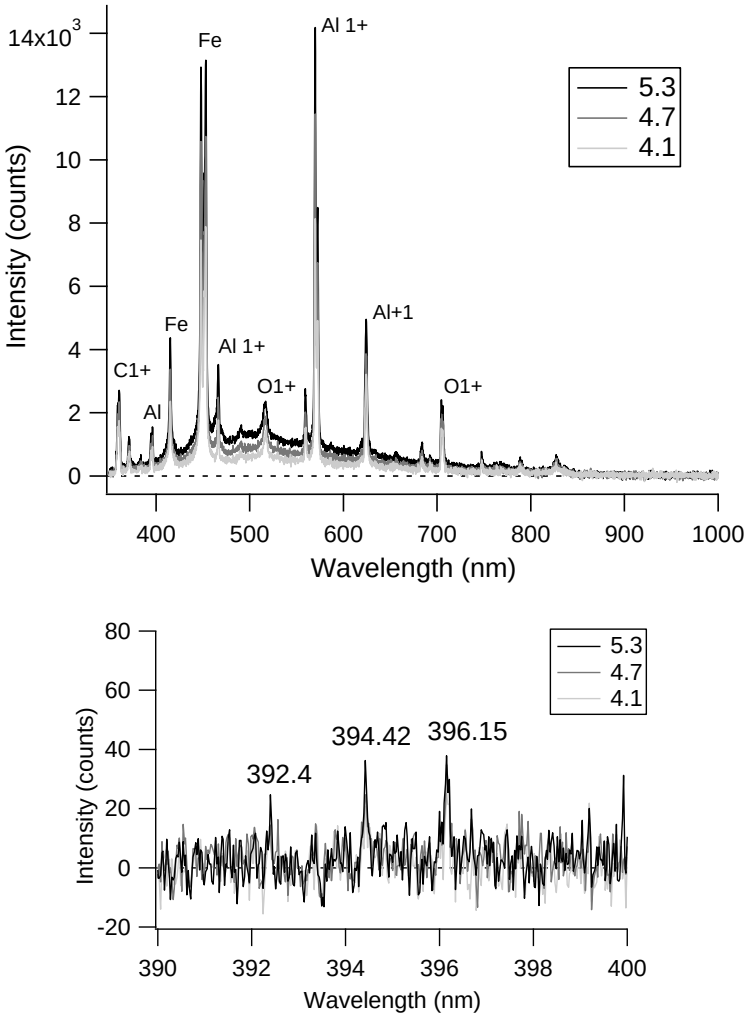

Figure 4.9 Optical emission spectra of the laser produced plasma using an aluminum hollow cylinder target for the broad band spectrum (top) and a high-resolution spectrum (bottom) from 4.1 to 5.3 GW/cm^2 laser power density.

4.4.2 Probe Signal Measurements

To characterize the plasma propagation out of the graphite target, probe current profiles shown in Figure 4.10 were measured for the laser power densities 8.9, 10.4, and 12.0 GW/cm^2 at 5 mm distance along the center of the target opening. At an 8.9 GW/cm2 laser power density, the positive signal had a peak at 0.25 A with the duration

of more than 0.5 μsec which became shorter but with higher peak current as the laser power was increased. By 12.0 GW/cm^2 laser power density, the probe current had twice the intensity for the positive signal and consequently a faster arrival time for the ions.

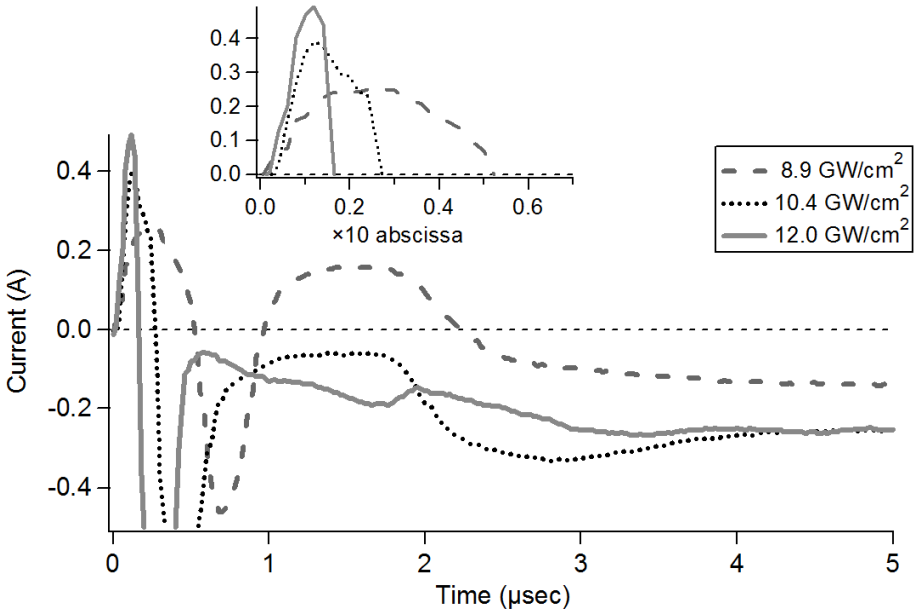

Figure 4.10 Probe current measurements 5mm in front of the target at laser power densities of 8.9, 10.4 and 12.0 GW/cm^2.

After thermalization in the hollow cylinder, plasma with high energy electrons effuse out to make the probe signal negative. The later part of the probe current profile after the initial positive peak displays a long stretch of negative signals caused by electrons and even slower ions. The plasma at the exit of the target eventually experiences a space charge neutrality in the later phase. The duration of the probe signal indicating charge neutrality extends to at least 40 μsecs. In the region, presence of low energy ions and formations of clusters are possible. This phase of the plasma

propagation requires further investigation to evaluate the composition of the laser induced plasma.

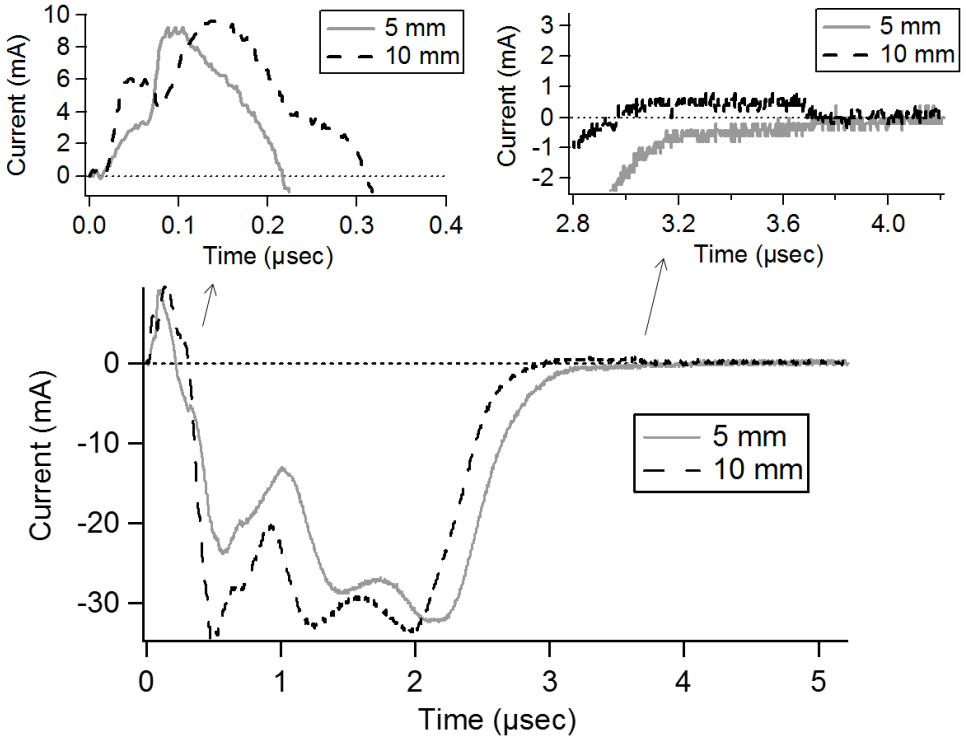

Figure 4.11 Probe measurements with distances of 5 and 10mm in front of the target at a laser power density of 10.4 GW/cm^2.

The space resolved probe signal measurements using two tungsten probes positioned 5 and 10 mm away from the target opening have shown how the plasma of each phase expanded to free space. A typical oscillograph trace shown in Figure 4.11 was taken for the laser power density of 10.4 GW/cm^2. Observations showed a delay of 0.1 μsec between the two probes which is caused by the probe location with 5 mm distance having a faster arrival of ions than the 10 mm distance for the positive part of the signal. Wider positive current profiles were acquired by the 10 mm probe distance than the 5 mm due to the propagation of ions from the target opening.

As the ions are transported further away from the target, subsequent collisions occur and increase the signal collected by the probe. The negative part of the signal starting from 0.5 μsec exhibited a reverse in the delay having a prolonged signal for the 5 mm probe distance compared to the 10 mm probe distance. The current profiles from the two probes were also identical varying only in magnitude with the 5 mm probe having less current and the time interval between the two signals was measured to be 0.1 μsec. In the overall signal, the magnitude of the negative portion of the signal was relatively larger than the initial positive peak and this negative signal extends up to 3 μsecs long. Looking carefully as the signal vanishes, the 10mm probe distance detected a slight increase in the positive signal before disappearing.

4.4.3 Langmuir Probe Analysis

Since the nature of plasmas formed through laser ablation occur at short durations in the range of microseconds, a fast sweep of voltage is needed to measure the current-voltage characteristics of the plasma. A frequency generator provided a 100kHz sinusoidal potential sweep which was amplified to have an $\pm$ 8 V peak-to-peak at the tip of the cylindrical tungsten probe. Located 15 mm away from the laser target exit, the Langmuir probe collected the ions from the carbon plasma that escaped the hollow target and the I-V curve is shown in Figure 4.12.

The current-voltage trace obtained from the measurements distinctly shows the ion and electron saturation regions. In the negative portion of the I-V curve, the ions collected in the probe gives a value for the ion saturation current of -0.5 mA. By plotting the natural logarithm of the difference of the probe and ion saturation current, the electron temperature can be calculating from the slope as given by equation (4.5). The electron temperature was calculated to be low with less than 0.5 eV. This is a good

indication of the low electron temperature condition of the plasma induced by the use of a hollow cylinder target geometry.

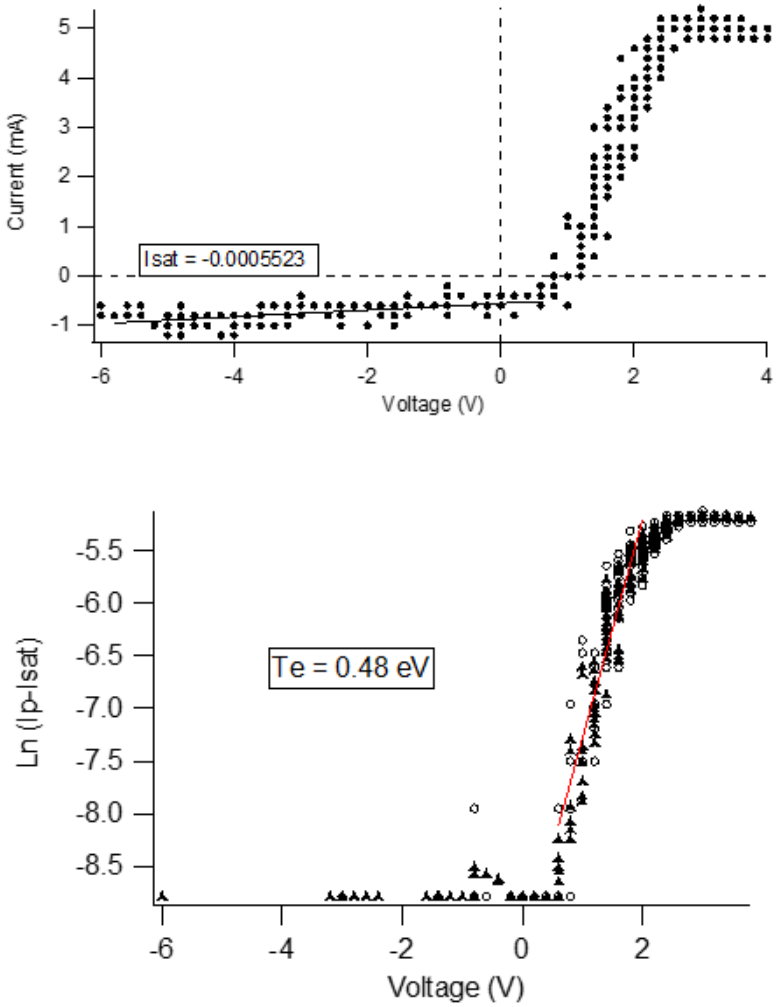

Figure 4.12 Current-voltage characteristics of the carbon plasma (top) and the calculated electron temperature (bottom).

4.5 Discussion

High speed images during the plasma expansion were captured for the graphite target with 10 mm and 7mm inner diameters. The front image perspectives showed the

inside of the target with the similar sequence of luminous cloud formation and expansion. However, the target with a smaller inner diameter had a copious amount of light emitting dust and particulates inside the hollow cylinder as compared to the other target design. This phenomenon is considered unfavorable to the plasma expansion as it indicates mass removal from the surface which is detrimental to the lifetime of the target. The side image perspective of the expansion area out of the target showed a noticeable difference to the shape of the bright plume. The target with the larger inner diameter design had the light of the plume concentrated intensely near the exit of the tube whereas the other target had a longer and more diffused afterglow. Reducing the dimension of the inner diameter by 3 mm significantly affected the propagation of the plume and the collision rate within the structure as indicated by the diminished intensity in the image.

Two target materials were also tested for the hollow cylinder design. High speed images with the front perspective to view inside the target observed the similar increase in light intensity at higher laser power densities. The cloud formation occurs at different laser power ranges with the graphite target needing more intense laser power to ignite the bright glow observed in the image. Since the plasma is produced through a thermal process, the thermal stability of the material is a major factor in the plasma ignition. With aluminum to be easily vaporized at a lower temperature than graphite, this implies the need for higher laser intensities to generate carbon plasma.

For the aluminum material, the optical reflectivity intensifies the light coming from the plasma and conceals the image. Using a 10 stop neutral density filter, images showed the small light at the center of the plume and as the laser power density was increased, a bright reflection appeared on the opposite wall. This light suggests the possibility of plasma formation on the adjacent surface for more intense laser

conditions. As the energetic ions coming from the laser produced plasma are accelerated toward another surface, this can cause sputtering of atoms which can be further ionized by the expanding plasma. The ionization of neutrals on the surface can also occur when the size of the plume gets larger at high laser power densities. On the other hand, the reflected light inside the hollow target was not observed in the high-speed images of the plasma for the graphite laser target.

The optical emission spectra of the plasma produced using the graphite and aluminum targets were measured to distinguish the ion species present in the plasma. As laser power density was increased, the emission lines observed in the spectra also grew in intensity without the appearance of new spectral lines. For the plasma using the aluminum target, aluminum as well as carbon, oxygen and iron ions were identified with single charge states and neutrals. The doublet charge state aluminum ion was also observed in the wavelengths 394.42 and 396.15 nm. As for the carbon plasma, carbon ions of up to C^{3+} charge states were identified in the spectrum.

Since the presence of higher charge state ions were detected in the plasma, the laser conditions need to be lowered during the operation of the laser ion source and reduce the plasma temperature. However, a continuum was observed in the background of the optical spectra both for aluminum and graphite material targets. This continuum is an indication of the thermalization occurring in the plasma by the spectral radiance. From Planck's radiation law,

$$u_{\lambda,T} = \frac{\hbar}{\lambda^3 \pi^2} \frac{1}{exp\left(\frac{\hbar c}{\lambda T}\right) - 1}$$

where u is the spectral radiance as a function of wavelength λ and temperature T. The background continuum corresponds to the spectral radiance of the thermalized plasma

with the peak of the distribution at 500 nm. This gives an estimate of the plasma temperature to be several thousands of Kelvin, implying a low temperature condition for the plasma.

To confirm the low plasma temperature observed in the optical emission spectra, the Langmuir probe analysis was performed on the expanding plasma. The ions were collected outside of the hollow target during the expansion phase of the plasma to take the measurement in a low plasma density region. The voltage sweep scanned at $\pm$ 8 V to give the I-V of the carbon plasma with the floating potential to be 0.8 V. The calculation for the electron temperature revealed to be less than 0.5 eV. This result agrees with the low temperature of the thermalized plasma from the optical emission spectra.

In the probe experiments for the plasma propagation, a single probe measured the current profile of the expanding carbon plasma at different laser power densities. Observations show broader peak signals for lower laser power densities and shorter durations as the intensity was increased. As the high energy electrons and ions collide with neutral atoms inside the hollow target and are partly thermalized before they escape out of the target.

The plasma inside the target relaxes with a time constant $\tau^{\alpha/\beta}$ between species α electrons and β ions which becomes smaller for more energetic charged particles which is given by,

$$\tau^{\alpha/\beta} = \frac{\upsilon^3}{\varepsilon_0 n_\beta L^{\alpha/\beta}}$$

where υ is the velocity, ε_0 is the permittivity of vacuum, nβ is the ion density and $L^{\alpha/\beta}$ is $m\alpha^2\upsilon^2/16\pi^2\varepsilon_0 e_\alpha e_\beta 2n_\beta \log \Lambda$ with log Λ as the Coulomb logarithm, more energetic

particles require more time to be thermalized.[28] This dependence of relaxation time against particle velocity explains the first part of the positive current signal, with higher duration for lower laser power. In the negative portion of the signal, it suggests the space charge neutrality occurring at the end of the signal. With electrons and slower ions contribute to the magnitude of the negative current measurement, the signal stretches on for several microseconds before disappearing.

For the double probe experiments, the delay between the two probe signals were analyzed. The first part of the signal was positive with the closer probe collecting the ions first the followed by the other probe with a wider positive peak. In the second part of the signal, the current becomes highly negative and the closer probe signal prolonged more than the farther probe. The reverse effect in delay is due to the faster decrease in the signal for farther distances from the source of ions as the low temperature plasma with high density rapidly diffuses in space. The positive signal corresponds to the positive floating potential or low plasma temperature, which is essential to negative ion production.

4.6 Conclusion

Plasma diagnostics were performed on the laser produced plasma to investigate the plasma conditions induced by utilizing a hollow cylinder target. Images were obtained using a high speed camera to examine the plasma formation and rapid expansion inside the target, and the directional propagation of a luminous cloud was observed in the images. The aluminum plasma images showed a reflected light on the opposite wall of the irradiated area for intense laser power conditions indicating the possibility of ionization of neutrals near the wall surface. Examining the side perspective images of

the graphite target shows a compressed plume as the inner diameter of the hollow target was reduced from 10 mm to 7 mm. In the optical emission spectra of the laser produced plasma, singly charged carbon ions and strong emission lines of up to C^{3+} charge states were detected in the carbon plasma whereas aluminum, carbon, oxygen and iron singly charged ions and neutrals were identified in the aluminum plasma. A background continuum was also observed for both target materials and plasma temperature was estimated to be below 1 eV. Langmuir probe signals were measured and the electron temperature was calculated to be 0.5 eV which agrees with the findings in the optical emission spectra. The probe current profiles were measured and the signals corresponding to positive ions were observed with faster arrival times for larger laser power densities. For more energetic ions inside the small volume of the target, the time needed for the plasma to thermalize inside the hollow structure became smaller which was exhibited in the first part of the positive current signal. The space resolved probe signal measurements showed a signal delay of 0.1 μsec between the two probes and a reverse effect in the delay occurred in the later phase plasma expansion. Information obtained from the plasma diagnostics on the laser produced plasma using the prototype laser ion source will be essential to further improve the system design for the continuous operation of the device.

Chapter 5

Rotating Hollow Cylinder Target Laser Ion Source

"The happy people are failures because they are on such good terms with themselves they don't give a damn."

-Agatha Christie

5.1 Introduction

In the development of ion sources, the intensity, ion species, efficiency, lifetime and stability specifications of the device determines the quality of the ion source.[29] To hold a wide variety of applications, these aspects of an ion source system need to reach a certain standard demanded by the specific application. The degree of success of the design depends on the performance of the system to produce the ions with the desired qualities. As an essential part of the development process, the prototype laser ion source system was assessed for the reliability of ion generation.

For initial testing stage of the hollow target laser ion source, the main characteristics of the laser produced plasma were investigated to verify the potential of utilizing a tube-type target structure as a new method to produce low energy ions. Using a modified laser target structure, the plasma from pulsed laser ablation did not expand freely in vacuum but was limited by the narrow volume of the hollow cylinder. This enabled the interaction of the plasma with the surface atoms of the target material

to cause the dissipation of energy through collisions. The experiments on the properties of the plasma showed the presence of low charge state ions including low electron temperatures as the charged particles exit the cylinder and drift to the downstream region. The effect of the geometric constriction to the expansion phase of the laser produced plasma can impede growth of high charge state ions and increase the probability of producing negative ions and even clusters.

While operating the prototype system during experiments, its performance as an ion source also showed some negative qualities that needs to be resolved. One major issue is the signal stability and the repeatability of the measurements. There is a significant decline in the measured signal intensity in Faraday cup signals or in probe measurements which will only allow for less than an hour for continuous operation using intense laser power. This immense drop in beam signal strength is due to the repetitive irradiation of the localized target surface. Since the hollow cylinder target is aligned inside the chamber and is stationary throughout operation, this degradation of the surface will tunnel through the cylindrical wall and reduce the operational lifetime of the laser target.

Stability of the ion source operation to function for long periods is essential for any system to be considered for work application. Maintaining and improving the efficiency of the system to function correctly ensures its reliability to meet the requirements of any specific purpose. For the prototype laser ion source, the important aspects of the system design that needs to be resolved is the beam current signal loss caused by repeated laser ablation. Allowing the laser beam to gradually strike another surface on the inner wall of the cylinder can extend the total working period before the surface gets depleted from laser erosion. A solution is the addition of a rotation mechanism to continuously turn the target during operation. This configuration will create a

uniformly eroded cavity inside the conduit due to the revolving mechanism as opposed to burrowing a hole on a fixed irradiated spot and should elongate the lifetime of the target usage.

The present chapter discusses the continuous operation of the laser ion source using the design of a rotating hollow cylinder target structure. To examine the stability, experiments were conducted continuously over a period assessing the improvements on the signal measurement as well as its degradation. To understand the beam profile, a travelling Faraday cup scanned the cross-section of the beam propagation. Using the new configuration of the laser ion source, the current profiles for the different laser power conditions were inspected to optimize the system operation.

5.2 Rotating Hollow Cylinder Target

The hollow cylinder target was designed to increase the collision rate during the expansion phase of the laser produced plasma by spatial constriction. With the intense laser irradiation on a fixed spot, deterioration of the surface progresses rapidly and continuous ablation leads to crater formation that eventually digs through the target. Figure 5.1(a) shows photos of the surface erosion on the hollow cylinder target due to continuoous laser irradiation. The repeated plasma expansion at a fixed location also forms an asymmetric surface on the inner walls of the cylinder since the intense exposure to the plasma is across the irradiated spot and this contributes to the signal fluctuations during measurements. To resolve the short lifetime and signal stability, a rotating mechanism was applied to the hollow cylinder target so that the irradiated spot constantly changes per revolution. The target assembly is shown in Figure 5.1(b)

where the rotating hollow cylinder graphite target with an inner diameter of 10 mm is aligned on the center of the axis with fabricated mechanical graphite gears to minimize the source of impurities for the carbon plasma production.

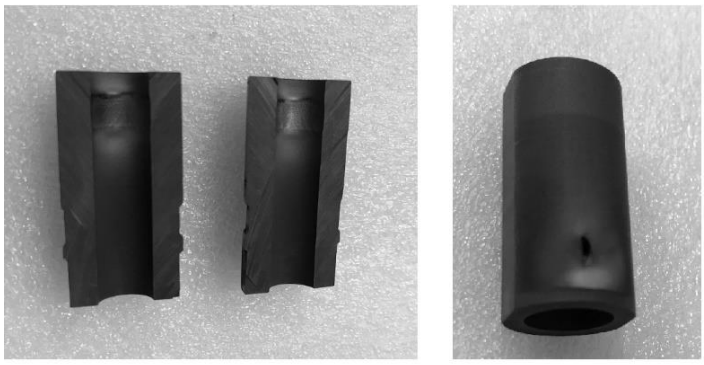

(a)

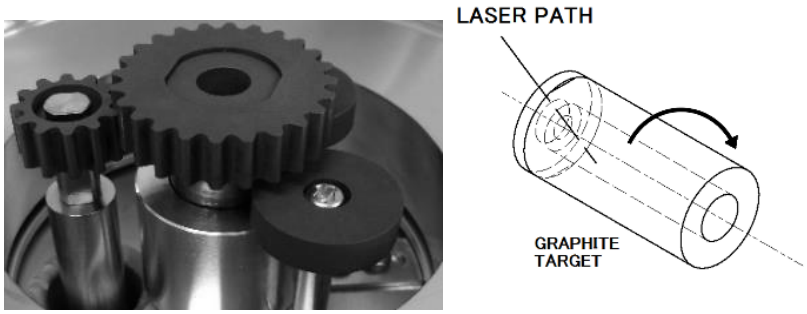

(b)

Figure 5.1 Images of (a) the eroded surfaces of the hollow cylinder target by repeated laser irradiation (b) the rotational mechanism of the hollow cylinder target.

To test the stability of the plasma pulses from the rotation of the hollow cylinder target, a 35 mm diameter Faraday cup measured the ion signals as the laser system was operated continuously at 10 Hz. The target with the rotational mechanism turned at a clockwise motion and a speed of 10 rpm driven by a stepper motor. The experimental

setup is shown in Figure 5.2 where an insulating flange separates the electrical connection between the hollow cylinder target side and the downstream chamber. In front of the graphite target exit, a grounded plate with a 10 mm hole aperture was placed 8 mm away to create a potential drop long the axis of the chamber. The ion signals produced by laser ablation using a laser power density of 13.5 GW/cm^2 was recorded for a period of one hour accumulating up to 36,000 laser shots. The progression of the ion signal in time was monitored to evaluate the operation using the new configuration.

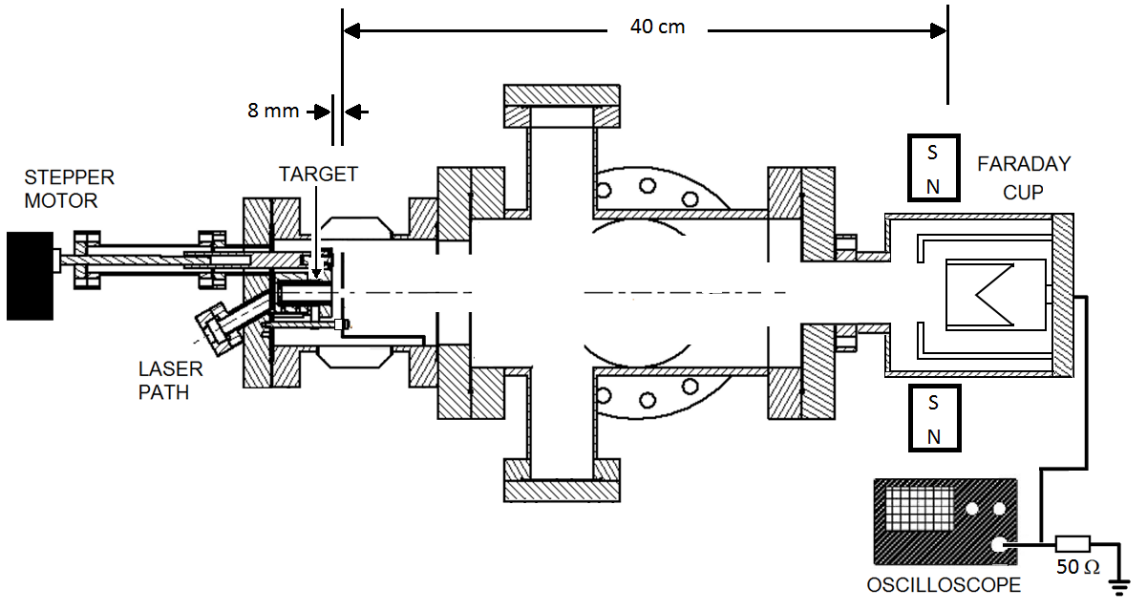

Figure 5.2 Experimental setup of the laser ion source with the rotational mechanism for the laser target.

The target material is also a factor to the rate of surface erosion caused by the laser ablation. The materials tested in the time evolution experiments are aluminum and graphite with both having identical dimensions of 10 mm inner diameter. Although

aluminum materials are irradiated at lower laser power densities than the graphite material, the intensity of the ion signal was adjusted using the laser power density so that the current measurements of the two materials will be in the same order of magnitude when performing the experiments.

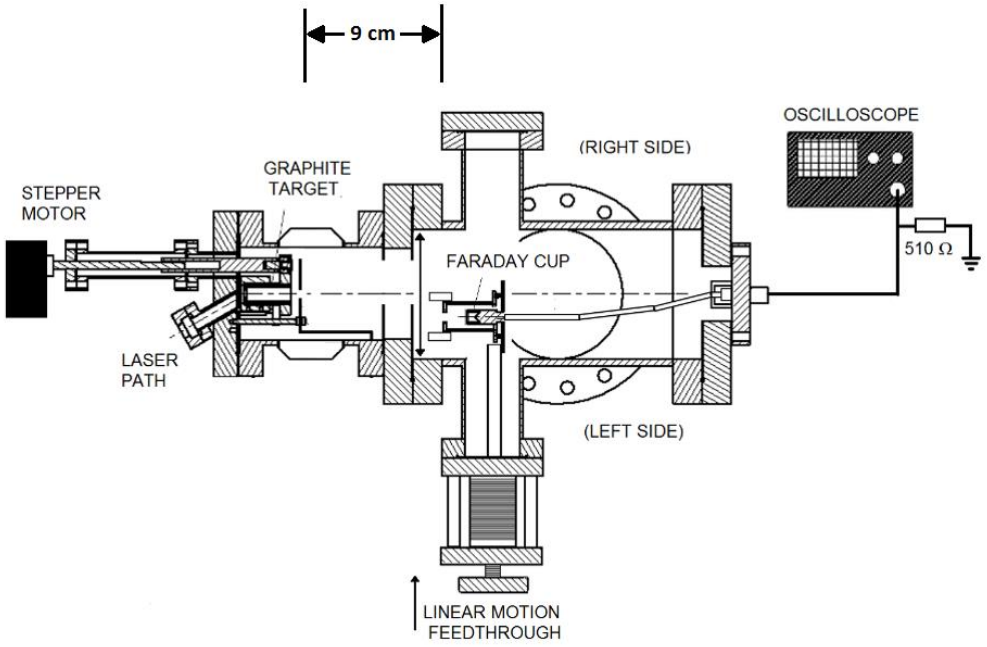

Figure 5.3 Schematic diagram of the laser ion source with the rotational mechanism and a travelling Faraday cup.

Aside from the time evolution experiments of the ion signals, the propagation of the charged particles flowing out of the hollow target was observed through a scanning a section of the ion beam. The schematic diagram of the laser ion source is shown in Figure 5.3 for profile scanning with the continuous operation of the system. A travelling Faraday cup was attached 9 cm away from the grounded plate to allow the measurement across the drift path. The cup collector was connected to a 15 pF 1 MΩ oscilloscope inputs with an external termination resistance of 510 Ω to enhance the

current measurements. Attached in front of a Faraday cup is a dipole magnetic configuration of 150 G along the axis to divert the incoming electrons and exclude it from the signal measurements. The beam profile scanned the cross section of the ion spread by moving the Faraday cup across ± 10 mm from the axis. The initial experiments will assess the performance of the laser ion source system moving towards a more efficient operation of the device.

5.3 Results

The experimental results are presented in this section, starting with the Faraday cup measurements of the plasma pulse. Th quality of ion production indicated through the signal stability are assessed for the continuous operation of the device. The beam current signals of the ion beam cross section and including the ion signals as a function of laser power density are explained for the current configuration of the laser ion source.

5.3.1 Time-evolution Experiments

The stability of the rotating hollow cylinder target was tested to compare the differences between the operation of a stationary target and the rotating configuration. The ion current measured in the Faraday cup shows a signal with a maximum peak current and the exponential decay of the signal. An example of a current profile from the Faraday cup is shown in Figure 5.4. The information extracted from the waveforms were the peak current and the time constant obtained from fitting an exponential function to the tail end of the signal. Those parameters were used to analyze the stability and reproducibility of the ion signals since the prolonged exposure to intense

laser diminishes the measured intensity and are easily reflected in the end of the waveform.

To interpret the time-evolution of the signal as the laser shots are accumulated in the target, the peak current is recorded along with the time constant of the signal decay. These measurements were made using the graphite target to observe the decline in the signal intensity for the two different laser ablation procedures. The waveforms were taken every 30 seconds for 1 hour of continuous operation. The peak value of the current signals and the calculated time constant for the two configurations are shown in Figure 5.4 as the laser output accumulated up to 36 000 shots.

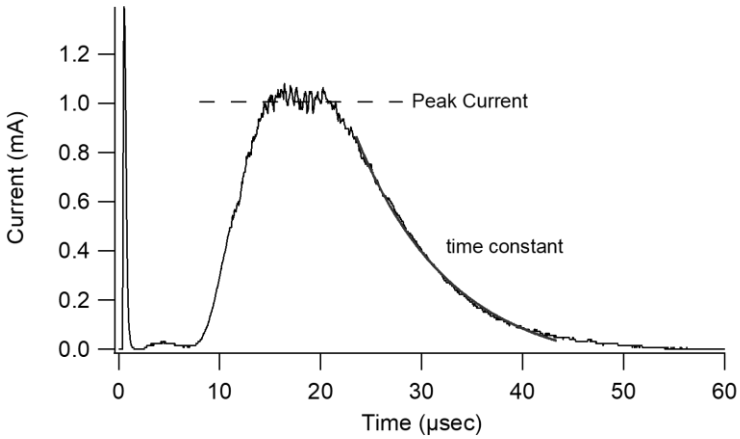

Figure 5.4 Ion current signal from the Faraday cup.

Although a linear decrease in the peak current of the rotating target is observed, the value of the current measurement for the stationary target decreased rapidly down to a (saturation) terminal value smaller by an order of magnitude; the peak current decreased from 0.5 to 0.05 mA after 25,000 laser shots of repeated irradiation. This shows the unsatisfactory performance of the laser ion source with a fixed or stationary target where it is difficult to maintain the current output at a certain level. For the

rotating target, the peak current started as dispersed but eventually converged over the course of 15,000 laser shots.

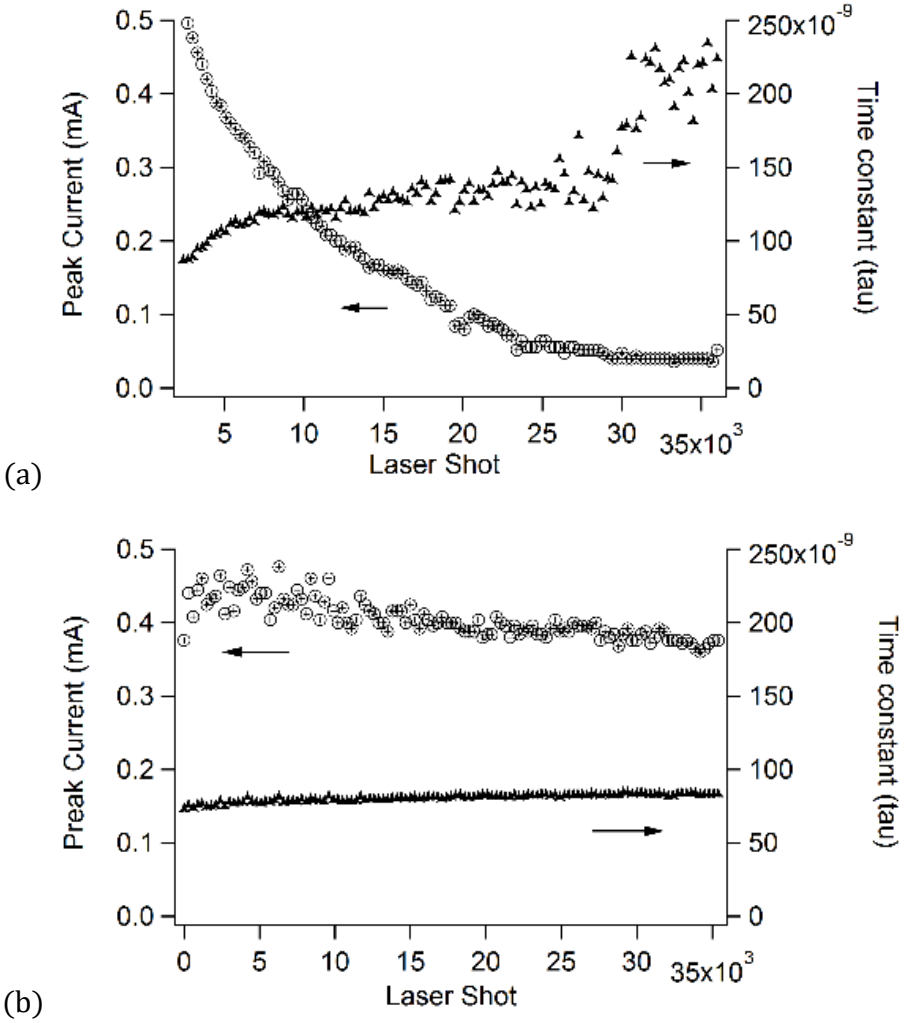

Figure 5.5 Comparison of signal stability for the (a) stationary and (b) rotating graphite target during an hour of continuous operation.

This may come from the unevenness in material surface during the first minutes of rotation. A slow increase in time constant for the stationary target is in agreement with the exponential decrease of the observed in the peak current. The rotating target

configuration on the other hand is showed even more constant characteristic and the time constant showed only a slight increase from 72.9 to 83.2×10^{-9} in values for the whole duration of the experiment. Physical inspection of the stationary target after the measurements revealed a deep hole through the cylindrical wall and affirm the lifetime of a fixed target configuration using a laser power density of 13.5 GW/cm^2 to be less than 1 hour.

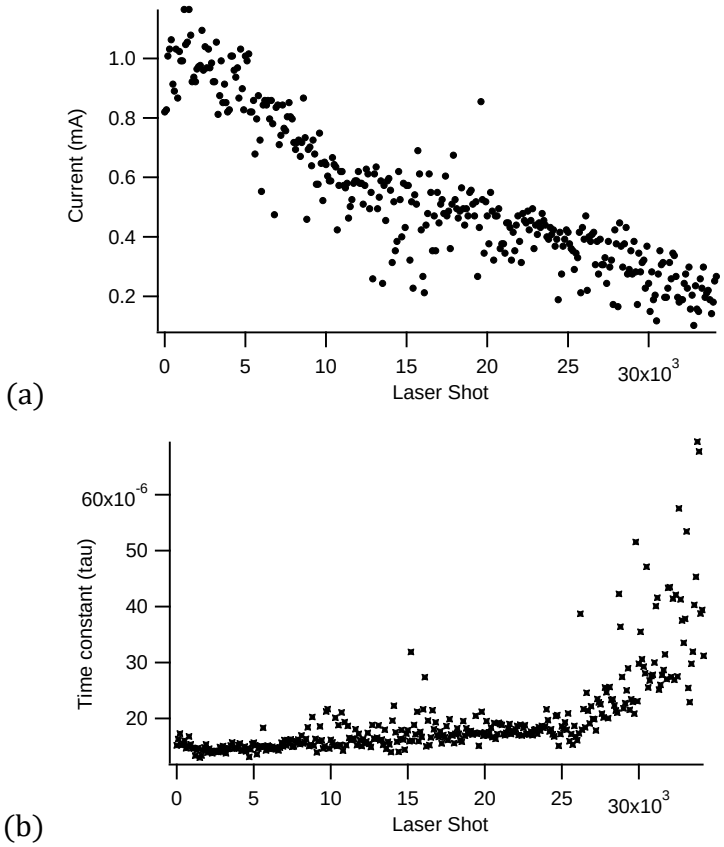

Figure 5.6 Signal stability of the aluminum hollow cylinder target for the (a) stationary and (b) rotating configuration during an hour of continuous operation.

The aluminum material was tested for the rotating hollow cylinder target using a laser power density of 5.3 GW/cm^2. The maximum current and the time constant of the signal decay is shown in Figure 5.5. Since materials with lower thermal stability are

more prone to erosion by laser ablation, the waveforms were recorded every 15 seconds for the duration of 1 hour to monitor the stability of the current peaks. The maximum values of the current profiles had a wide spread as observed in Figure 5.5(b) and slowly decreased from a 1 mA to 0.2 mA. The time constant however was increasing but suddenly grew steep after accumulating over 25,000 shots. The stability of the ion signals of the aluminum are not as constant as the graphite target with the current values fluctuating at 0.9 mA within the first 5,000 laser shots before declining in signal intensity.

5.3.2 Time-of-flight Analysis

Scanning the time-of-flight signals at different locations across the drift region using the graphite target will give an image of the beam spread at 9 cm from the grounded plate. Shown in Figure 5.6 is the Faraday cup measurements at $\pm$ 10 mm on the beam cross section with the negative notation indicating the left side and positive for the right side of the chamber. There are two peaks observed in the wave signal. The sharp positive burst for the first peak showed an arrival time of at 0.5 μsec and a pulse width of 0.1 μsec. Experiments were made to investigate the origin of the signal and based from an unaffected time signal even with an accelerating fields of 2 kV potential difference, this was infered to be photon induced current signals from the plasma. The second signal was determined to be the ion signal coming from the the laser produced plasma that arrives at a later time of 5 μsecs.

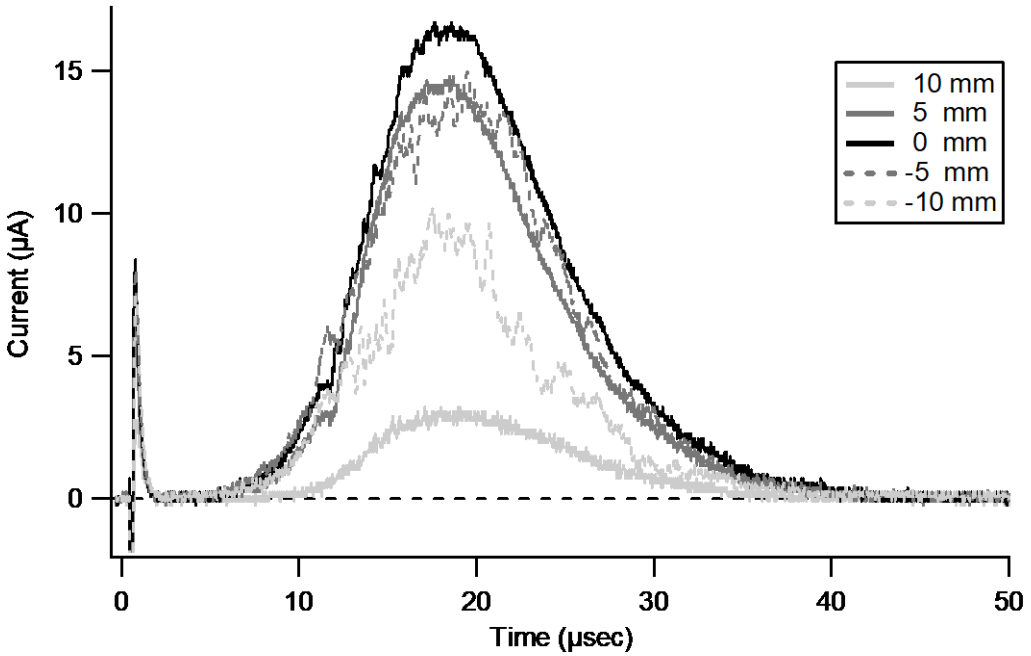

Figure 5.7 Time-of-flight measurements from a graphite target across the ion propagation region from the left(negative) to the right(positive) side of the chamber.

The measurement of the ion current shows the maximum peak along the axis and slowly decreases as the Faraday cup is moving away 10 mm from the center. The cross section of the beam reveals a symmetric profile of the ions as it moves away from the cylindrical target. Within the 10 mm range on the center, the large part of the ion signal was observed and crossing over more than 5 mm from the center immediately reduces the current magnitude. The signal on the right side dropped to one fourth of the maximum magnitude whereas the left side decreased by half.

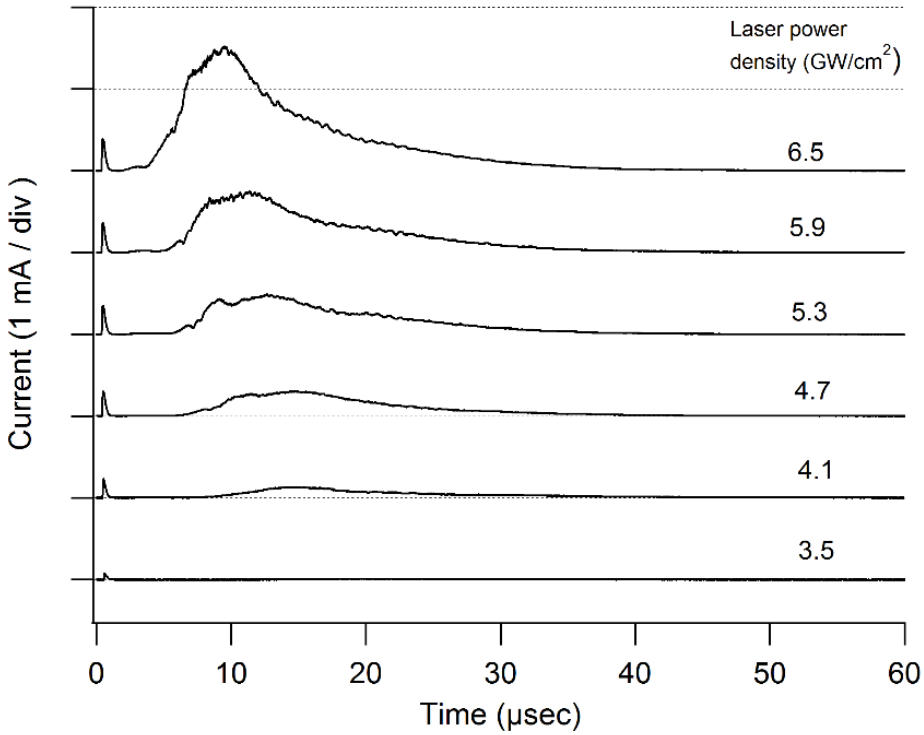

Figure 5.8 Ion signals as a function of laser power density for a hollow cylinder graphite target.

Inspecting the ion signals from the laser produced plasma will help set the optimal parameters for operation. Using a graphite target, the time-of-flight measurements from 3.5 to 6.5 GW/cm^2 laser power density is shown in Figure 5.7. Observing the waveforms at a lower laser power regime shows the minimum laser parameters to generate an adequate amount of ion signal. At 4.1 GW/cm^2 laser power density, a weak signal is observed with an arrival time of 8 μsecs and current intensity of 0.1 mA. As the laser power density is increased, the signal arrival time is faster indicating a higher plasma temperature that requires less time to generate ions. Examining the current profiles, the ion signals using intense laser power also shows a narrower distribution which is caused by the presence of more energetic ions. The maximum current

magnitude observed in the experiment is at 1.4 mA using a laser power density of 6.5 GW/cm^2.

The time-of-flight measurements for an aluminum target is also examined using the same laser power density range of 3.5 to 6.5 GW/cm^2. A noticeable difference is the laser power density requirement of the aluminum target material being less than the graphite target where an ion signal could be detected for the laser power density of 3.5 GW/cm^2. The signals however contain a large number of electrons which is reflected as a negative signal in the profile. The maximum current values for the laser power densities 5.3, 5.9 and 6.5 GW/cm^2 are all in the same order of 2mA. As signal arrival time becomes faster for more intense laser energies, examining the fast parts of the signal at higher laser intensities reveals fast signals with an arrival time of 3 μsec when the laser power density exceeded 5 GW/cm^2. The appearance of fast signals that correspond to energetic ions are only generated when the laser intensity reaches a minimum energy for ion production.

Aside from the difference in current intensity from the aluminum and carbon laser produced plasmas, one important parameter is the rise time of the signal. The signal rise time reflects the plasma temperature from the laser ablation. The mass of aluminum and carbon are very different, with 27 and 12 amu respectively. Considering the large distribution in the spectrum, the aluminum has a long rise time of 19 μsec for the laser power density of 4.7 GW/cm^2. Comparing it to the graphite target with the same laser conditions, the ion current from the carbon plasma has a smaller intensity but the plasma temperature is higher as suggested by the signal rise time of 6 μsec. One reason is due to the abundance of electrons for the aluminum plasma which can cause shieling when it interacts with the electromagnetic fields. This implies the efficiency in photon absorption and ionization for the graphite target.

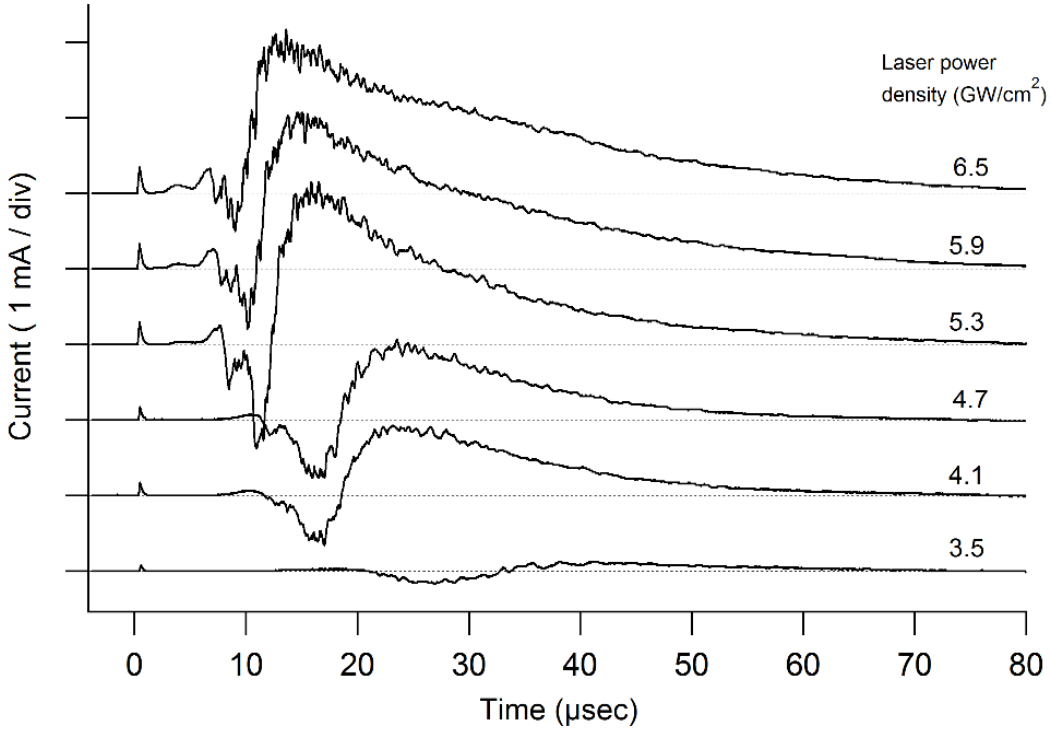

Figure 5.9 Ion signals as a function of laser power density for a hollow cylinder aluminum target.

5.4 Conclusion

To improve the stability of ion production of the laser ion source, a rotating mechanism was employed to the hollow cylindrical target allowing the continuous operation of the device. The system using the rotating hollow cylinder graphite target showed an improvement in signal stability compared to stationary targets. Aluminum materials for targets however are weak toward the successive laser irradiation as the current intensity declined over an hour of operation. The Faraday cup scanning across the beam cross section showed a symmetrical profile with the ion signal concentrated

at $\pm$ 5 mm from the axis. Time-of-flight measurements for aluminum and graphite targets were examined and observed the development in the current signals as the laser power density was increased up to 6 GW/cm^2. The signals using the graphite target had lower intensities than the aluminum target but the plasma temperature was observed to be higher. Fast signals corresponding to energetic ions appeared in the onset of the ions signal for the aluminum target at high laser power densities. Additional studies on ion mass separation will be conducted to determine composition of the laser produced plasma.

Chapter 6

Mass Spectrometry of the Laser Produced Plasma

"I never expect to see a perfect work from imperfect man."

-Alexander Hamilton

6.1 Introduction

When developing ion sources, the ability to produce specific ion species for a particular field displays the pervasiveness of a device to the technology of ion sources. Fundamental information about to the capabilities of the laser ion source determine its quality and reliability as a device that can be applied to many disciplines. For the hollow cylinder target laser ion source, the system is in the early development stage where laser ablation using a non-planar target is being demonstrated. The next phase is to verify the ions that can be generated when utilizing a unique target structure.

In the previous chapter, the intensity, lifetime and stability of the laser ion source was evaluated for the continuous operation of rotating the hollow target. The results shown in chapter 5 for the Faraday cup measurements display the plasma expansion from graphite and aluminum hollow cylinder targets with intensities proportional to the laser power directed to the surface. Although the generated ions from the conventional laser ablation yield similar ion current profiles, the expansion process is

fundamentally different since the confined region containing the expanding plasma should induce ion-atom collisions rather than the adiabatic expansion to free space. The transfer of kinetic energy from the energetic ions to the surrounding atoms can be described as a cooling effect which can lead to interesting results for the produced ion species, charge states and including the formation of neutrals through sputtering or recombination.

The ions generated from laser ablation are studied through their time-of-flight and the results will be discussed in this chapter. By creating an electrostatic field to accelerate the charged particles, the ions that leave the hollow target will attain different velocities that are based on their charge-to-mass ratios. As the ions drift to a travelling distance, the arrival times will vary which are then detected by the Faraday cup. Calculating the mass from the current peaks that correspond to the ions gives an estimate of the species that are produced in the laser ion source. This analysis for the mass separated ion signal is essential to confirm the generated ion charge states as well as the possibility for atomic cluster formation.

In another ion beam diagnostics system, the laser ion source using a graphite material for the hollow cylinder target was tested for the correlation of the ion signal intensity and drift distance as measured by movable a Faraday cup. For laser ablation using planar targets, the dense plasma expansion to the surrounding space which occurs three dimensionally.[30] This plasma expansion is defined by,

$$T \propto L$$

and,

$$I_{peak} \propto L^{-3}$$

which is the relation of the drift length L to the ion beam pulse width T, and peak current I. The properties of the expansion permit the scaling and estimation of the

plasma parameters at certain locations along the drift region. Although the mechanism is different for laser produced plasmas using a hollow cylinder target, the space-resolved current measurements will verify its disparity to the conventional transverse expansion from a planar target.

Using the same system configuration, an electrostatic ion analyzer with a bending radius of 90° separated the ion signals which were detected by a secondary electron multiplier. The charge-to-mass ratios were calculated from the time-of-flight of the generated positive ions from the hollow cylinder target. This gives a good estimation of the ion composition in a single plasma pulse.

6.2 Theoretical Considerations for the Time-of-flight Analysis

The velocity of an ion or a singly charged particle with a relative mass M is described by the equation,

$$v_i = \sqrt{\frac{2\varepsilon}{M_i}}$$

where ε is energy of the ion which is given by the elementary charge and the extraction potential, $\varepsilon = e\Phi$. [31-32]

As the charged particles are extracted from an ion source, the velocities of those ions can vary depending on the ion mass of the species. Illustrated in Figure 6.1, the ions drift along a distance and arrive at different times, faster for light or more energetic ions and longer drift time from larger or massive particles.

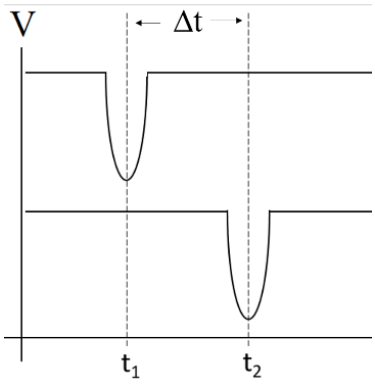

Figure 6.1 An example of a time-of-flight signal for two ions with different masses.

In the time-of-flight spectral analysis, a particle with a given velocity υ is moving to a certain distance L at a given time t. This relation is often defined by the basic equation,

$$t = \frac{L}{v} \quad .$$

For a drift distance of 40 cm, the ion velocity would then become,

$$v_i = 1.39 \times 10^6 \sqrt{\frac{\varepsilon\,[V]}{A\,[amu]}} \qquad [^{cm}/_{S}]$$

so that,

$$t = \frac{L}{v} = 28.8 \sqrt{\frac{A}{\varepsilon}} \qquad [\mu sec]$$

which will give the time-of-flight of an ion with a given extraction voltage ε and atomic mass A. Now, consider two signals that correspond to a single ion of an unknown mass, the difference in their arrival time Δt for a drift distance is,

$$\triangle t = t_2 - t_1 = \frac{L}{v_2} - \frac{L}{v_1}$$

and since the ions have different energies,

$$\triangle t = \frac{L}{\sqrt{\frac{2\varepsilon_2}{M}}} - \frac{L}{\sqrt{\frac{2\varepsilon_1}{M}}}$$

$$= \frac{1}{\sqrt{2}} \frac{\sqrt{\varepsilon_1} - \sqrt{\varepsilon_2}}{\sqrt{\varepsilon_1 \varepsilon_2}} \sqrt{M}\ L$$

$$= \frac{1}{\sqrt{2}} \frac{\sqrt{\Phi_1} - \sqrt{\Phi_2}}{\sqrt{\Phi_1 \Phi_2}} \sqrt{\frac{A\, m_A}{e}}\ L\,.$$

The time Δt in seconds for a drift length of 40 cm is,

$$\triangle t\ = \frac{\sqrt{\Phi_1} - \sqrt{\Phi_2}}{\sqrt{\Phi_1 \Phi_2}} \sqrt{A}\ \ 8.26 \times 10^{-11}\ .$$

If the extraction voltages are set at 1 and 2 kV, the potential Φ_1 and Φ_2 will result to an equation for the mass in amu,

$$A = \frac{\triangle t^2}{1.63\ \times 10^{-12}}$$

for a potential difference of 1 kV between the two ion signals.

6.3 Mass Analysis Experiments

The mass separation of the ions from the laser produced plasma are performed to determine the ion species produced using the hollow cylinder target. The ions are extracted from the carbon and aluminum plasmas to investigate the charge states of the ions as well as the possibility of atomic clusters. The ion signals including the calculations for the mass based from the time-of-flight are discussed in this section.

6.3.1 Experimental Setup

In the ion extraction experiments for the mass separation of charged particles, an illustration of the ion source system is shown in Figure 6.2. A 0.5 mm thick aluminum grounded plate with a circular aperture of 10 mm in diameter was placed 8 mm in front of the target. The motor driven rotation of the hollow cylinder was as slow as 10 rpm with the target flange electrically insulated from the main vacuum chamber. A high voltage source supplied to the target region created a potential drop of up to 6 kV to effectively accelerate the ions. Given a drift distance of 40 cm, the Faraday cup with a magnetic filter of 150 Gauss to suppress electrons collects the mass separated ion signals. The ion extracted signals were obtained with the sequence starting from a high voltage potential of 6 kV and decreasing down with 1 kV increments. The Faraday cup collected the ion current and was recorded in averaged waveforms by an oscilloscope using a 50 Ω termination resistor.

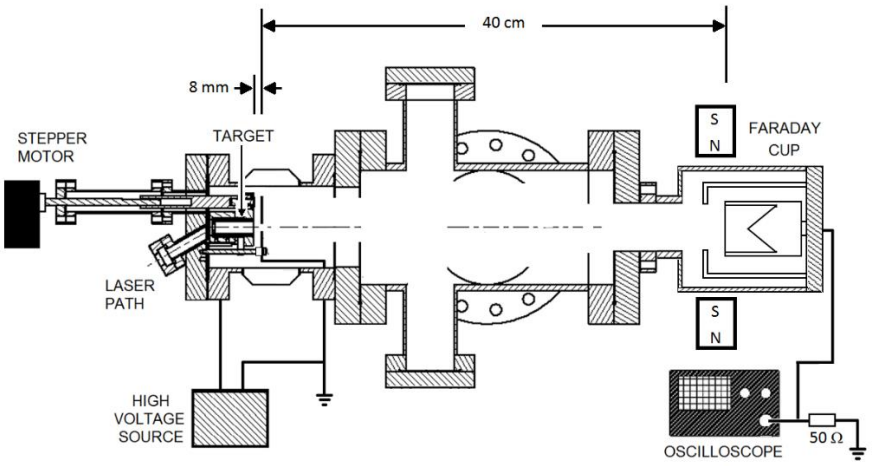

Figure 6.2 Illustration of the laser ion source for time-of-flight analysis.

The extraction of ions was performed for the two laser target materials, aluminum and graphite, to examine the ion species produced from laser ablation. Since the laser

power density requirement to produce plasma is lower for aluminum targets, the laser was operated to have 4.1 GW/cm^2 for the aluminum target and 5.3 GW/cm^2 for the graphite target to minimize the ion current intensity for well mass separated signals. By estimating the mass based on the velocity induced by the accelerating field, the mass spectrum of the ion species through the time-of-flight measurements will estimate the composition of the laser produced plasma.

6.3.2 Results

The initial mass separated signals of the ions from a graphite laser target are shown in Figure 6.3(a). where the termination resistor in the oscilloscope was set to 510 Ω. Applying a potential difference of up to 5 kV, the current peaks are observed which shows the different ion signals drifting with different velocities. The large current profile arriving at 15 μsec for 1 kV extraction potential is retarded in time and intensity as the voltage was increased and disappeared at 3 kV and higher. Slow ion signals that arrive at 13.36 μsec and 11.23 μsec are observed at 1 kV and arrives faster as the extraction voltage is increased to 5 kV. Attaining faster velocities with greater extraction potentials, the ion signal peaks eventually overlaps and become difficult to distinguish. The appearance of some small current peaks was also observed when the voltages reached 3 kV.

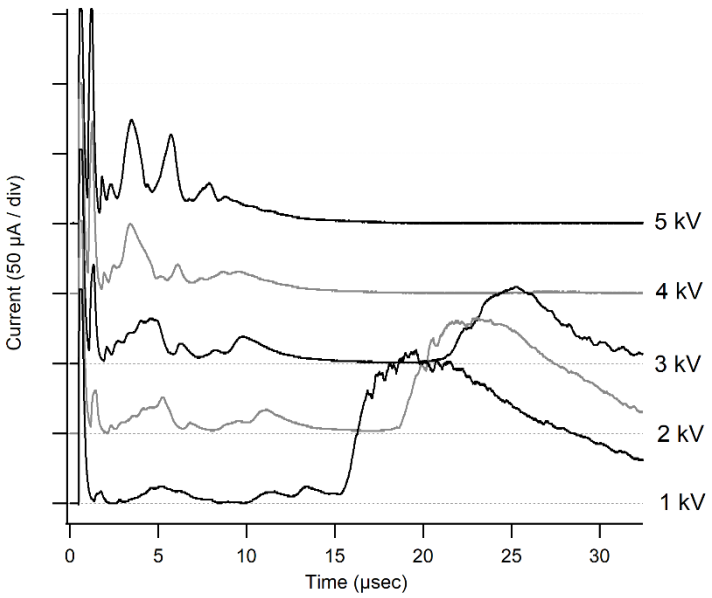

(a)

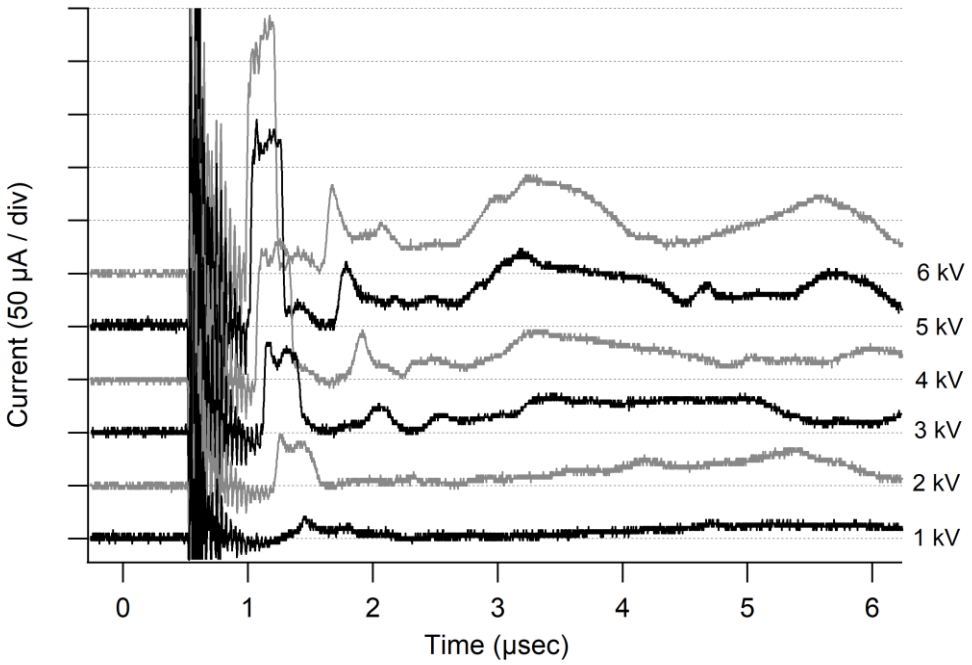

(b)

Figure 6.3 Ion signals from the laser produced plasma using the graphite target with a (a) 30 µsec and (b) 6 µsec time range.

For time-scales less than 10 μsec, the current peaks gather together when the accelerating field becomes greater. Due to this effect, current measurements are taken again with different conditions of up to 6 kV extraction potential which can improve the signal along with using a 50 Ω termination resistor. The mass separated spectrum is shown in Figure 6.3(b) having the range of up to 6 μsec. The initial positive burst that correspond to the photon induced current at the onset of the plasma formation, shows noise that originates from transient signals and its signal reflection in the coaxial cable. Examining the ion signals arriving after 1 μsec, the signals shows clear ion current peaks which signify the arrival of light or energetic ions.

The first signal that is detected has a 1.46 μsec signal arrival time and with a 5 kV potential difference, it had a faster arrival time of 1.06 μsec with a 0.4 μsec time difference.

During the analysis of the current signals, it is important to note that the recorded waveforms were triggered to the q-switch signal of the laser system which implies a time delay from the moment laser strikes the surface. By using the photon induced current from the onset of the current signal, the time of arrival of the first ion peak is then 0.94 μsec for 1 kV and 0.52 μsec for 6 kV extraction voltage. The second current signal detected in the spectrum appeared when the potential was at 3 kV. The identified current peak had a faster signal with also a 0.4 μsec time difference which confirms the uniform acceleration applied to the ions by the electrostatic field.

The mass separation of the ions generated from the laser produced plasma for the case of aluminum is achieved through the use of an electrostatic accelerating field. The broad time-scale of the current measurements of up to 60 μsec is shown in Figure 6.4(a). Similar to the current peaks from the carbon plasma, a large signal at the end of the spectrum that arrives around 30 μsec was observed with retarding in time and

diminishing in intensity as the extraction potential rose to 3 kV and disappears at higher voltages. The ion signals measured revealed very slow current peaks with the slowest arrival time of 26 μsec and with faster arrival time of 14 μsec at 6 kV showing a 12 μsec time difference. The following ion signal exhibited a broad peak with a width of 10 μsec which narrowed as the extraction was set to higher potentials.

To accurately identify the peaks, a higher resolution time-scale ranging up to 12 μsec was recorded to clearly examine the ion signals. The time-of-flight spectrum is shown in Figure 6.4(b) for a shorter time-scale. The waveforms observed the fastest ion signal arriving at 1.7 μsec with the current peak increasing with the extraction voltage but the arrival time having a 0.24 μsec time difference with the 5 kV potential difference between 1 to 6 kV.

The next ion signal only appeared when the extraction potential was at 3 kV and the current peak had an arrival time of 3 μsec. Other peaks could be identified in the current measurement however, the signal appeared to be broad. The signal arrival times of the succeeding current peaks were 4.6, 5.5 and 6.5 μsec for a 2 kV extraction potential. This can still give a proper estimate of the mass of the ions as indicated by the time-of-flight signals. Similarly, a photon induced current signal could be seen in the beginning of the time-of-flight signal. The indication for the plasma formation can be assumed to be at the same time as the photon signal which starts at 0.5 μsec. The arrival times of the ion signals need to be adjusted accordingly to provide a more precise estimation of the ion mass.

Since aluminum ions are relatively heavier than carbon ions, the drift time of the ions are slower as compared to carbon. The signals obtained also included less noise from signal reflections in the coaxial cable. With the identified signals from the

measurements, the mass based from the ion signals can be estimated to understand the ion composition of the aluminum plasma from the hollow cylinder target.

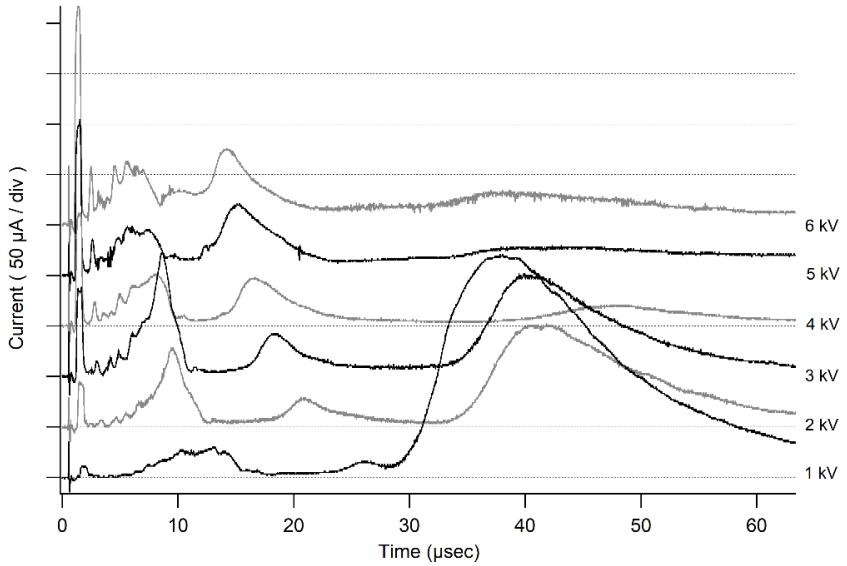

(a)

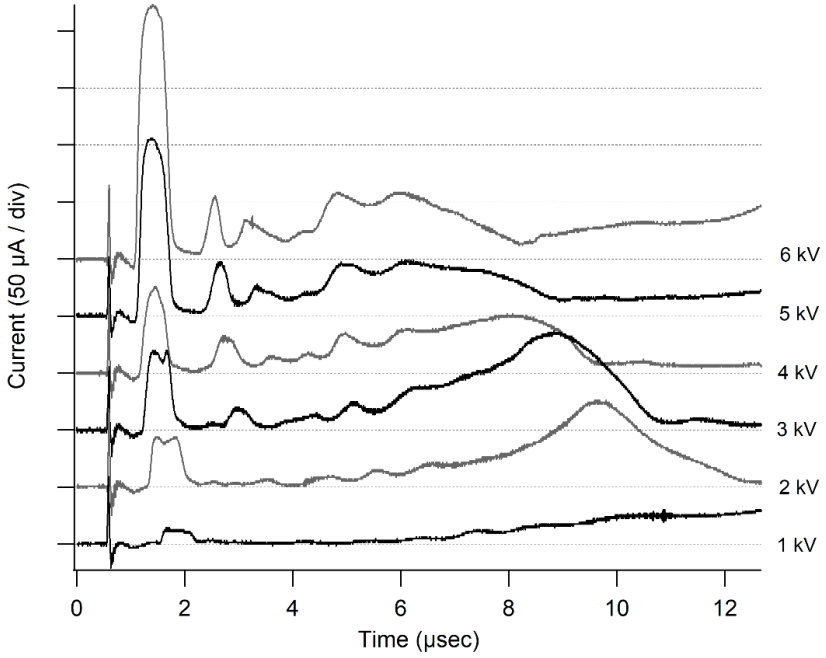

(b)

Figure 6.4 Ion signals from the laser produced plasma using an aluminum target with a (a) 60 μsec and (b) 12 μsec time range.

6.3.3 Discussion

The current signals with peaks relating to the mass separated ions are identified from the time-of-flight. The initial burst found on the current measurements for both aluminum and graphite is an indication of the plasma ignition as the current signal was induced by the photons coming from the plasma. This gives an offset of 0.5 μsec in all of the signals and set the initial time t_0 to this point. Before analyzing the data, it is important to recall that the ions initially have a velocity obtained from expansion phase of the plasma and then accelerated by electrostatic forces. Since the laser produced plasma already has a self-extracting property, the total energy of the ions would then be,

$$\boldsymbol{E_{total}} = E_{expansion} + E_{extraction} \quad .$$

This would explain that the detected ion peaks should have faster arrival times than the estimated calculations of the time-of-flight.

First, for the carbon plasma, the measurements show recognizable peaks that shift to faster arrival times alongside increasing the energies applied in the ion extraction. The first signal for the 5 kV extraction potential arrived at 1.06 μsec and applying the offset will shift the time to 0.5 μsec. The ion signal appears to be broad that suggests a collective of energetic ions with overlapping drift times. As observed from the previous chapters, the ion species observed in the carbon plasma showed the presence of carbon charge states of up to C^{+3} based from the optical emission lines. Calculating for the time-of-flight of carbon ions for charge states 2 and 3 result to a time of flight of 0.91 and 0.75 μsec. Since the ions detected in the Faraday cup have a background velocity coming from the plasma expansion of the laser ablation, it is possible that the first ion peak signal in the measurement are the high charge state carbon ions.

Shown in Table 6.1. are the calculated and observed ion flight times and the corresponding ion species. Based on the signals in the longer time-scales of the Faraday cup measurements, slow and massive ions could be detected suggesting the formation of clusters in the laser produced plasma. The slowest current peaks arriving around 8 μsec for the extraction voltage of 5 kV estimated to be caused by particles of atomic mass in the range of 450 amu. The identified peaks revealed the presence of carbon clusters of C_2, C_4 and C_{16} as approximated through their mass. The massive ions showed to be small fullerites of C_{24} and C_{36} detected at the tail end part of the current measurements with their current peaks even visible at lower extraction voltages. The possibility of forming clusters in the laser ion source suggest the mechanism of the hollow cylinder target as a means to induce agglomeration of atoms that can eventually lead to producing fullerene cages.

Table 6-1 Peak values of the time-of-flight signals and the possible ion species.

Observed peaks	Offset corrected	Possible Species	Calculated TOF
1.01	0.50	C^{+2}, C^{+3}	0.91, 0.75
1.66	1.15	C_1	1.28
2.05	1.54	C_2	1.81
2.97	2.46	C_4	2.57
5.72	5.20	C_{16}	5.60
7.52	7.00	C_{24}	7.72
8.74	8.22	C_{36}	8.46

For the aluminum plasma, the current signals show both fast and slow peak arrivals extending up to 26 μsec for a 1 kV extraction potential. The first recognizable peak arrives at 0.79 μsec with for the extraction potential of 5 kV and can also we

observed in lower potentials. The ion signal measured possibly corresponds to the singly charged aluminum with the atomic mass of 13. Calculating the time-of-flight for the particular ion results to a 1.34 μsec arrival time. Although the difference between the calculated value and the signal measurement is 0.5 μsec, this can also be a consequence for the initial velocity of the ion making the total energy higher than the calculations.

Table 6-2 Peak values of the time-of-flight signals and the possible ion species.

Observed peaks	Offset corrected	Possible Species	Calculated TOF
2.48	1.91	Al	1.93
3.11	2.54	Al_2	2.7
4.80	4.23	Al_5	4.32
5.93	5.36	Al_8	5.46
9.26	8.69	Al_{20}	8.64
14.2	13.63	Al_{52}	13.93

The formation of aluminum clusters has been observed for pulsed laser ablation, hence, it follows that the slow and massive signals can be from the agglomeration of aluminum atoms. The signals indicate the presence of Al, Al_2, Al_5, and larger aluminum clusters of Al_8 and Al_{20} for the slower arrival time of the peaks. The time-of-flight signal found at 14.2 μsec suggests the possibility of a large aluminum cluster of Al_{52} where the atomic group structure pertains to a magic number sequence for stable cluster formation. Although, the presence of oxygen and other impurities can contribute to the formation of other kinds of molecular clusters, the mechanisms for the aluminum cluster formation under laser ablation conditions needs to be confirmed.

From the singly charged aluminum and carbon ions are detected from the ion current signals, it shows the energy growth of the ions as the potential difference was increased. As previously mentioned, the energy of the ions is due to the potential applied to the extractor and the initial velocity coming from the expansion of the laser produced plasma. It is possible to deduce the initial velocity of the ions prior to extraction from the time-of-flight signals. To examine the progression of the ion energies relative to the extraction potential, a graph of the arrival time of the signals for singly charged carbon and aluminum ions is shown in Figure 6.5. The plot of $1/t^2$ gives a linear relation to the extraction potential which shows that for less energetic ions the drift time becomes larger reducing the value of $1/t^2$ to zero. As the extraction potential approaches zero, the ions energies should also diminish assuming that the ions started at rest. However, in the case of laser produced plasmas, the absence of extraction potentials means that the ions are simply expanding freely to self-extract with a given energy. The energy was estimated to be 0.5 keV as the linear plot for singly charged aluminum and carbon ions were extended to $t = 0$. This approximation agrees with the previous diagnostics experiments where that the temperature of the plasma is relatively low and the ions should have energies less than 1 keV.

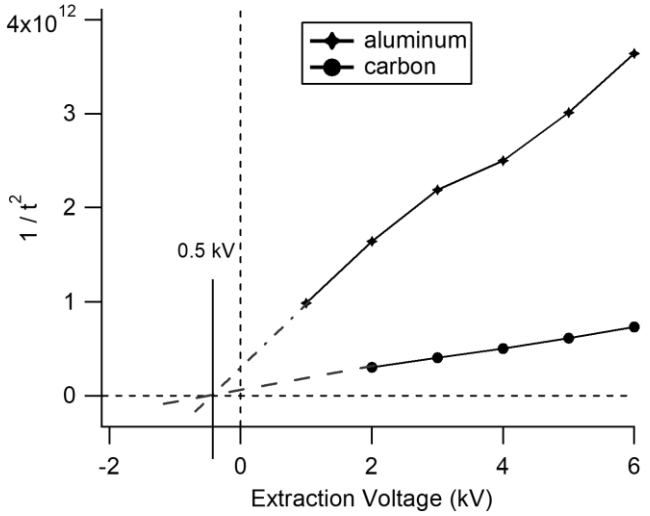

Figure 6.5 A graph of $1/t^2$ versus the extraction potential for single charged aluminum and carbon ions.

6.4 Rotational Hollow Cylinder Graphite Laser Ion Source

Experiments were conducted to investigate the plasma from a hollow cylinder target using the beam diagnostics system developed for the laser ion source in Brookhaven National Laboratory. The characteristics of a laser produced plasma from a hollow cylinder target was examined to understand the expansion principle and its similarities to conventional planar type laser ablation. Aside from space resolved Faraday cup measurements, a 90° electrostatic ion analyzer coupled to a secondary electron multiplier analyzed the ion composition in the pulsed plasma. The positive ions generated in the ion source were identified through the charge-to-mass ratios for the different ions.

6.4.1 Experimental Setup

The laser ion source system has a beam diagnostics system to study the laser produced plasma through the use of a Faraday cup and an electrostatic ion analyzer are aligned along beam axis. The collector for the Faraday cup has a 40 mm diameter opening with a mesh guard operated at -1 kV to exclude the electrons from the measurement. The pressure of the vacuum system during the experiments were in the order of 10-4 Pa to eliminate the possibility of recombination as the ions expand transversely.

For the laser conditions, an intense pulse of a 1064 nm laser beam is focused using a condenser lens to a spot size of 0.17 cm^2 with an incidence angle of 30° on the target surface to achieve a laser power density in the range of 10^8 W/cm^2. The Q-switch delay of the laser is adjusted to control the laser power of the output beam and experiments are performed with the laser power density of 2.0×10^8 W/cm^2. The configuration of the beam diagnostics for the space resolved Faraday cup measurements are shown in Figure 6.6. Using a linear motion feedthrough to adjust the location of the Faraday cup, measurements were taken along the beam axis for the distances of 60 to 90 cm from the target exit. The waveforms were recorded using an oscilloscope with a 50 Ω termination resistor and the signals were triggered to a photodiode that captured the light from the laser pulse.

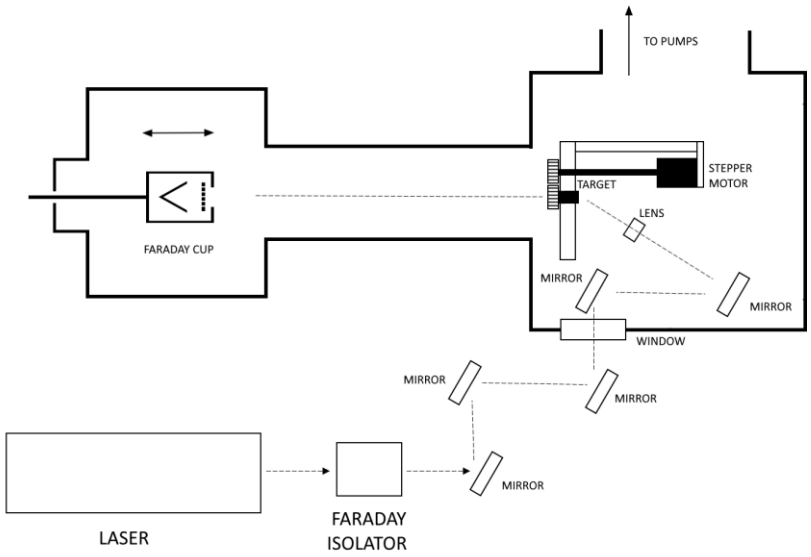

Figure 6.6 Experimental setup of the rotating hollow cylinder target for the space resolved Faraday cup measurements.

The other set of experiments includes an electrostatic ion analyzer where the ions are bent to separate the ion signals which are then detected by a secondary electron multiplier. The experimental diagram for the experiment is shown in Figure 6.7. The measured waveforms from the experiments were averaged to verify the stability of the signal. Along the same axis, a secondary electron multiplier coupled to an electrostatic ion analyzer is placed 3.86 m away from the target. The ion trajectory is deflected 90° with a radius of curvature of 100 mm using an electrostatic field and an electrode spacing of 5 mm. A slit width of 0.02 mm at the front and 4.8 mm at the back of the deflection electrodes was used for mass separation. The secondary electron multiplier collects the ion signals with the ion species determined through the time-of-flight of the different charge-mass ratios. In front of the electrostatic ion analyzer, a retractable Faraday cup at 2.4 m from the target measures the voltage profile of the plasma before

and after the mass separation to check the reproducibility of the measurements. The electric field in the cylindrical electrodes is varied accordingly to change the ion trajectories and allow selected ions to pass through. Those signals are processed to provide an estimate of the composition ions species in a single plasma pulse.

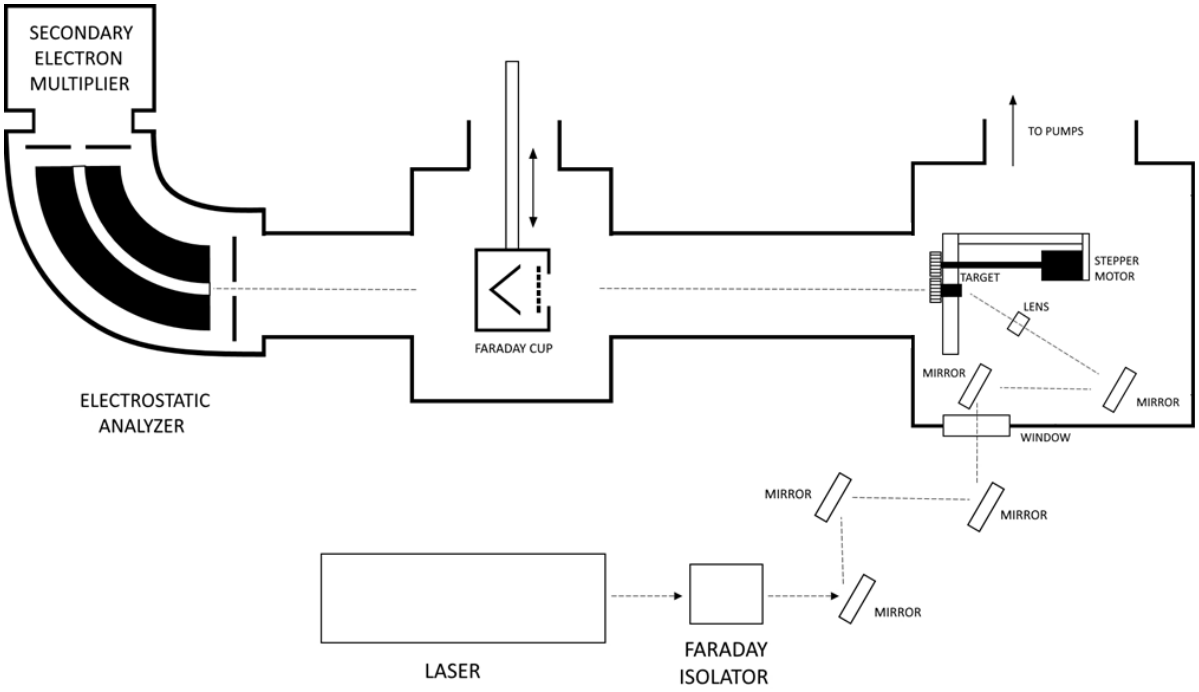

Figure 6.7 Experimental setup of the rotating hollow cylinder target for the ion mass analysis.

6.4.2 Space-Resolved Faraday Cup Measurements

When an intense laser strikes the planar surface, it forms a dense plasma which expands longitudinally and transversely. The transverse propagation the ions have been observed for different drift lengths and led to formulating the relation between the ion peak intensity and the drift distance. Although the basic principle of the plasma formation is almost identical, the conditions of plasma expansion are entirely different

since the propagation is limited by a cylindrical volume before escaping to the ion source chamber. The expansion of the plasma in a hollow cylinder target is also not perpendicular to the irradiated surface but at a glancing angle. This difference in the conditions of plasma expansion are examined for the case of a hollow cylinder target to see if the scaling relation is valid.

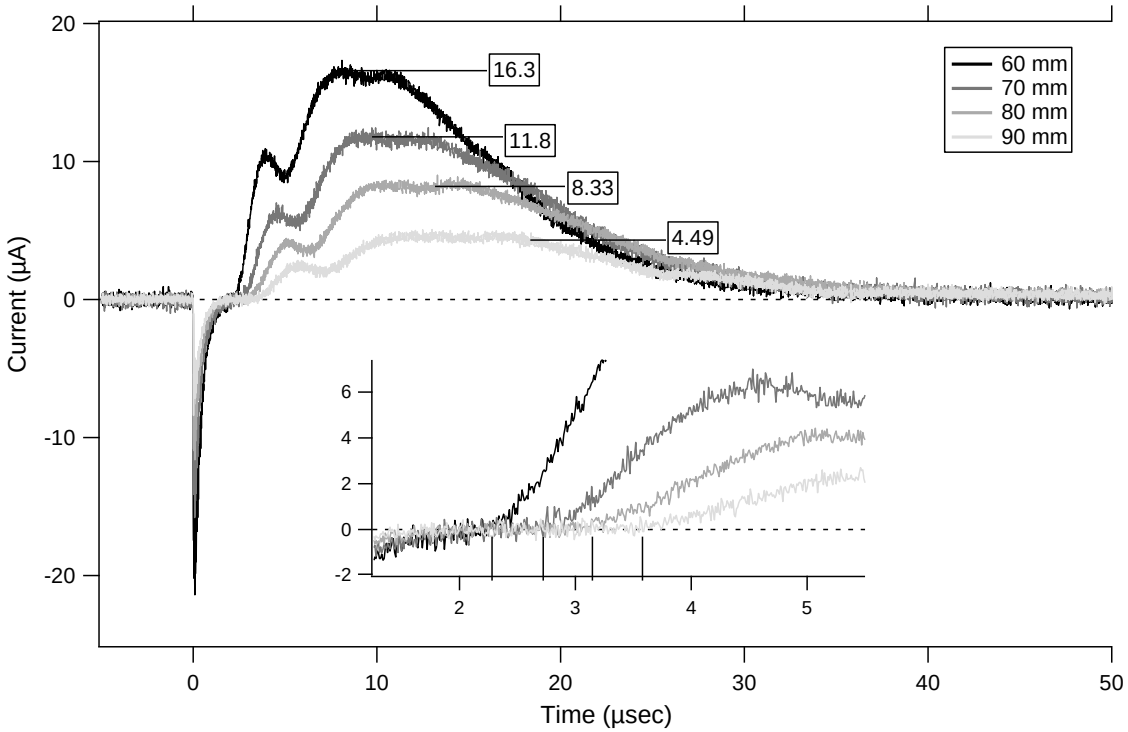

Figure 6.8 Space resolved Faraday cup measurements for the laser produced plasma using a hollow cylinder graphite target.

Examining the onset of the signal, a sharp negative peak is observed prior to the positive distribution that corresponds to the plasma pulse. A similar burst is found in the previous chapter where the Faraday cup measurement recorded a positive peak which was due to a photon induced signal to the ion collector. Since the Faraday cup assembly used in this experiment utilizes a negatively biased grid as an electron

suppressor, the electrons produced from the photons coming from the plasma are redirected back to the collector due to the external electric field which creates a negative signal instead. Following the negative peak, the ion signal of the plasma pulse arrives after 2 μsecs with a delayed risetime of 0.25 μsec for every 10 cm distance away from the target. The Faraday cup measurements for the distances 60 to 90 cm along the axis exhibits a proportional relation to the pulse width of the signal. On the other end of the signal, the tail end extended further for a total width of almost 50 μsec seen in the pulse duration at a 90 cm distance. This elongation of the current measurement displays a broadened ion signal for far distances along the axis.

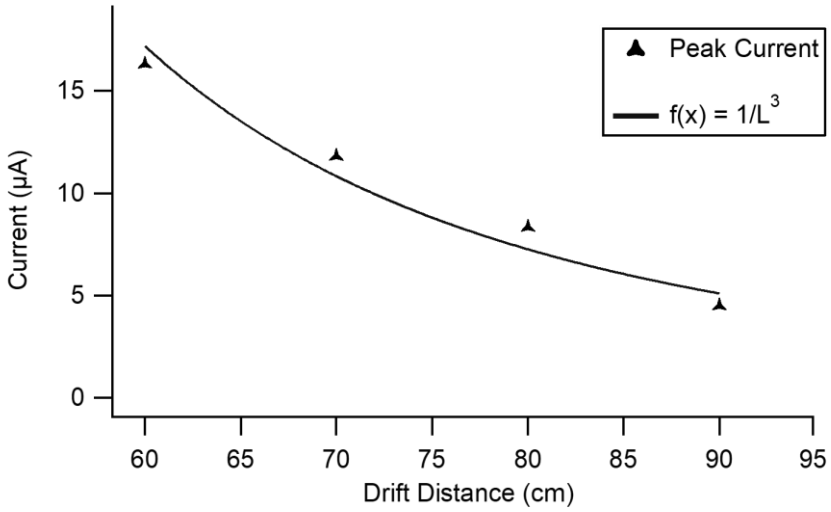

Figure 6.9 Space resolved Faraday cup measurements for the laser produced plasma using a hollow cylinder graphite target

At a distance of 90 cm, the intensity dropped to 25 % from the 16.3 μA down to 4.49 μA. At farther distances from the source, the solid angle of the measured signal becomes smaller which is reflected by the intensity. However, for laser produced plasmas using planar targets, the peak current is proportional to the drift distance by

L^{-3}. A plot of the peak current against the drift distance was made to test the validity of that relation for the case of a hollow cylinder target shown in Figure 6.9. The L^{-3} function displayed alongside the peak current graph shows that the same relation applies for the hollow cylinder target. Although measurements are conducted over a range of only 30 cm for the drift distance, this scaling system can apply to even farther locations along the axis but are limited as the distance grows closer to the plasma source where the particle density is high and the charged particles do not diffuse independent of each other.

6.4.3 Electrostatic Ion Analyzer Experiments

In the experiment to separate the ions through electrostatic deflection, the current profiles of the plasma pulse were first inspected by the retractable Faraday cup measured the waveforms to confirm the signal stability during operation. The ion signals for the plasma pulse were recorded before and after the mass analysis experiments. The voltage measurements were fluctuating and a conditioning period of continuous ablation for 5 seconds was employed allowing the laser to vaporize the target surface evenly as it was being rotated. The averaged waveforms are shown in Figure 6.10 have a signal duration of 200 μsecs and decreased from 192 to 153 μA of the voltage peak after the ion mass separation experiments. The distributions are almost identical for the two waveforms except for their peak intensities. This indicates that the mass analysis performed is comparable to the plasma pulse being observed by the Faraday cup signal having minimal changes in the time-of-flight.

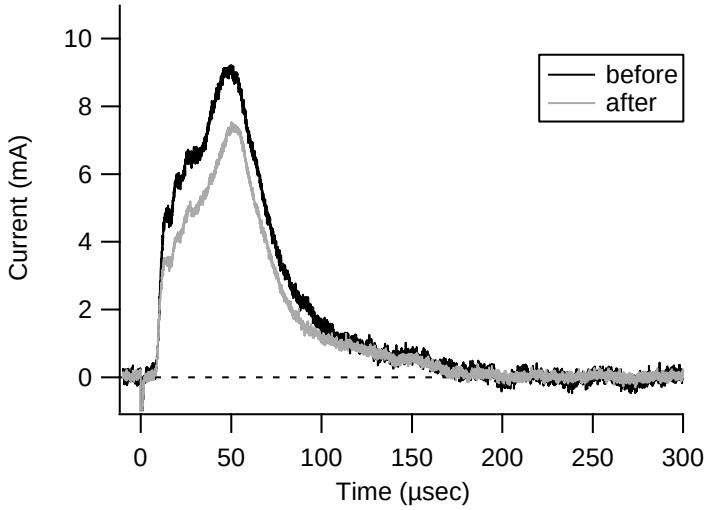

Figure 6.10 Averaged ion signals before and after the mass analysis experiments.

As the electric field along the cylindrical electrodes are adjusted, ions with a specific trajectory dictated by their charge-to-mass ratio pass through the analyzer. The secondary electron multiplier measures the incoming ions and obtains the time-of-flight spectrum. As the elecrostatic ion analyzer scans through ion energies, the ion species are identified to estimate of the composition of the plasma pulse. The raw time-of-flight signals operated at voltages 4, 10 and 15 V. are shown in Figure 6.11. The voltage peak with an arrival time that matches to the singly charged carbon ion are observed in the spectrum as labeled in the graph. Increasing the voltage of the electrode allow the ions to arrive faster, the signal intensities remain only in a small energy range before disappearing. This enables the mapping of the detected ions throughout the period of the pulse.

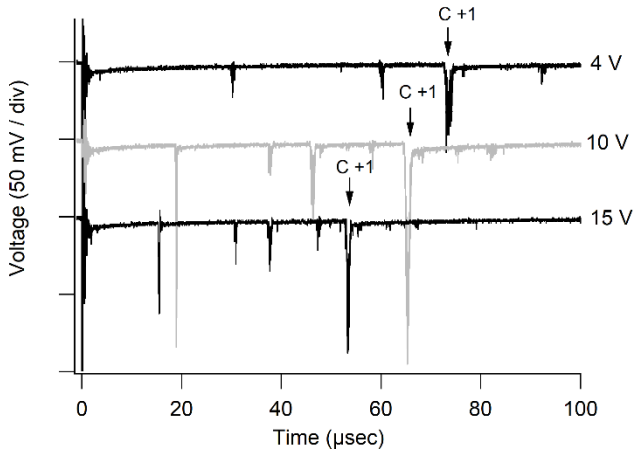

Figure 6.11 Averaged ion signals before and after the mass analysis experiments.

Positive carbon ions with charge states of up to +3 and H^+ ions are distinguished from the ion analyzer as the electrode voltages were varied from 1.5 V to 80 V. Based on negative peaks of the identified ions, the magnitude and arrival times were recorded over a range of input voltages in the ion analyzer. The data processed gave the total ion current for the specific ion species and this recreates an ion voltage distribution similar to the one obtained from the Faraday cup. The graph of the ion current for the different ion species are shown in Figure 6.12 to see the components of the plasma pulse. The initial portion of the ion signal comprises of the high charge state carbon ion C^{+3} along with lighter ions such as H^+ and singly charged carbon ions including C^{+2} make up the tail end of the distribution. Since ion currents are divided according to the ion species in the plasma, it follows that integrating the everything should give the total ion signal depicted in the Faraday cup measurement. It is important to remember that the measurements from the secondary electron multiplier and the ion signals from the Faraday cup were obtained at different locations. This means the pulse width and intensities should also be different. Given that the relationship between the drift

distance and the ion peak intensity have been verified for the case of hollow cylindrical targets, the assumption for a scaling technique can be applied to the measurements for a more accurate comparison.

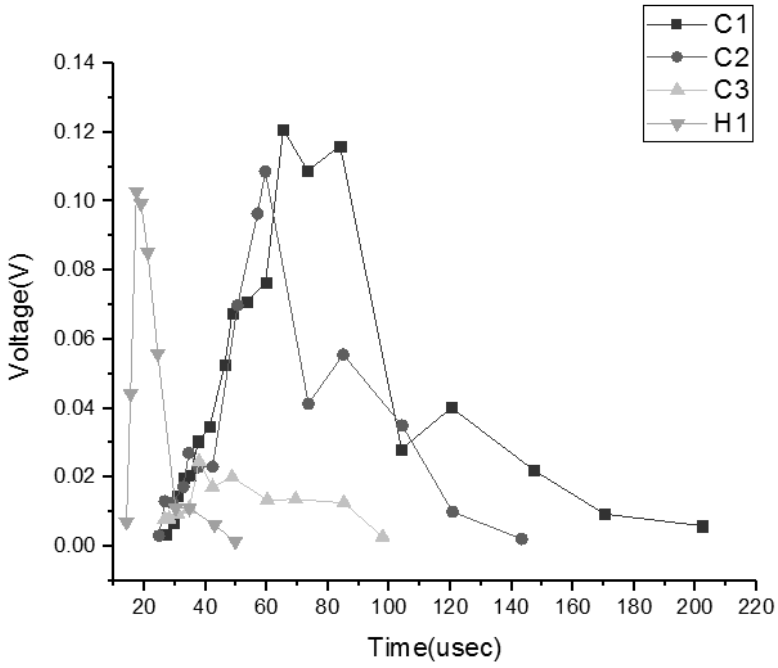

Figure 6.12 A graph of the detected ions peak signal arrival times.

Completing the analysis on the ion signal, the measurements are all scaled to the distance of the Faraday cup at 2.4 m away from the hollow target. This will ensure proper comparisons of the measurements taken at different locations. The graph shown in Figure 6.13 includes all the signals of the ion species, the integrated signals from the secondary electron multiplier and a Faraday cup waveform after the ion analysis experiments all scaled at 2.4 m away from the target. This presents a proper representation of a single plasma pulse using the hollow cylinder target. Comparing the integrated signals to the Faraday cup measurement, the distribution is very similar this asserts the validity of the estimation on the ion composition in the plasma.

Inspecting the profile of the Faraday cup measurement shows the peak of the distribution reflects the abundance of lower charge state carbon ions C^{+1} and C^{+2} in the plasma based on the mass separated ion signals. This shows that the plasma pulse mainly comprises of low charge state ions which is an indication of the low temperature condition of the laser produced plasma. However, a small high energy component was observed in the initial portion of the plasma. This comes from hydrogen as observed in the graph where the signal comes from the adsorbate layer of hydrogen on the surface of graphite which is regularly replenished from the surroundings as the plasma dissipates. This effect can be observed as hydrogen are detected again during the continuous operation of the pulsed laser.

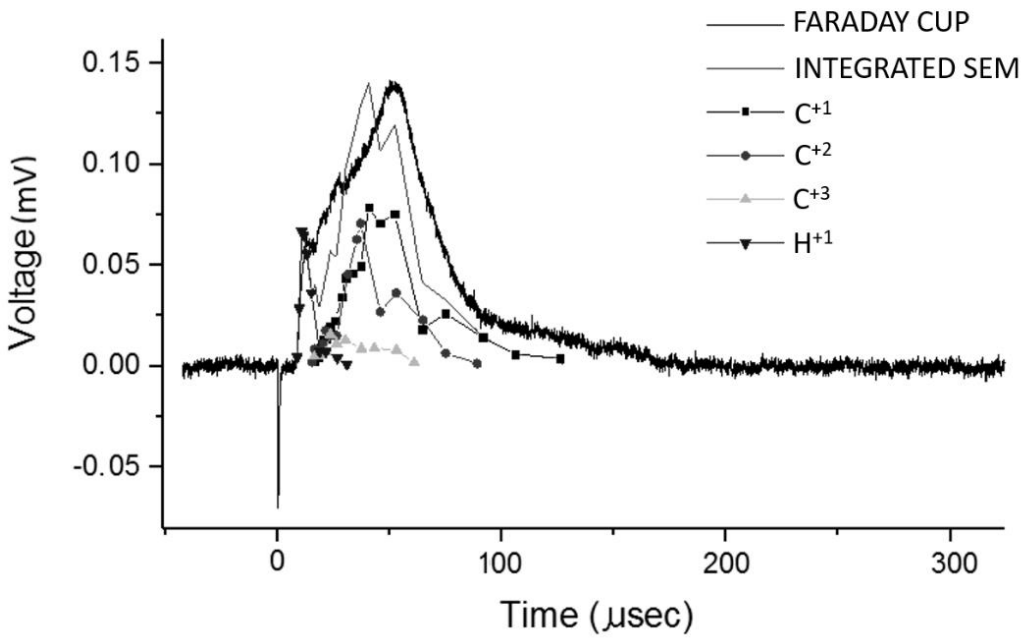

Figure 6.13 Ion signals of the Faraday cup, the ion species and the integrated signals from the secondary electron multiplier all scaled to the location at 2.4 m away from the hollow target.

6.5 Conclusion

Experiments were performed using a hollow cylinder target in the laser ion source system to identify the ions species generated in the plasma. This section covers two experiments from two different beam diagnostics system. Positive ion extraction experiments were performed for the targets with graphite and aluminum materials. Signals that correspond to massive ions were identified for both materials and suggest the possibility of cluster formation. Carbon clusters of small fullerite, C_{24} and C_{36} clusters were recognized from the time-of-flight measurements. Aluminum clusters were also identified and massive ions of Al_{20} and Al_{52} were detected in the measured signal peaks. While the ions are extracted at high potentials, ions from laser produced plasmas already possess an initial velocity that come from the expansion phase of the ablated plasma. This was energy was estimated to be 0.5 keV for both of the singly charged aluminum and carbon ions.

The second set of experiments investigated the relationship between the drift distance L and the ion peak currents for the case of hollow cylinder targets. The proportionality relation of the current to L^{-3} was verified from the space resolved faraday cup measurements. The relation was applied to process the data obtained from the electrostatic ion analyzer. The ion species distinguished from the time-of-flight signals were C^{+1}, C^{+2}, C^{+3}, and H^{+1}. The signals were scaled using the relation between the current, time and the drift distance to estimate the ion composition in a single plasma pulse. This revealed that plasma pulse is mainly composed of the low energy ions, C^{+1} and C^{+2} but also including a small portion of C^{+3} and H^{+1}. This follows that the laser produced plasma pulse realizes the low temperature condition of the plasma as indicated by the abundance of singly charged ions.

Chapter 7

Conclusions

"Biologically speaking, if something bites you it's more likely to be female."

-Desmond Morris

7.1 Main Results

This dissertation describes the development process of a new type of laser ion source and demonstrates the operation of laser ablation using a hollow cylindrical target. The idea of applying a geometric constraint to the expanding laser produced plasma aims to reduce the plasma temperature by increasing the ion-atom collisions. This has led to the design of the modified hollow target structure and the assembly of a laser ion source.

For the prototype design for the laser ion source, the experiments on the prototype system showed images of the plasma formation inside a hollow cylinder target for the first time. Measurements using a Faraday cup to obtain the ion current profile detected the arrival of electrons followed by the ions which displays their mobility during free expansion. Plasma diagnostic experiments were conducted to investigate further the characteristics of the plasma through plasma spectroscopy and probe signal

measurements including Langmuir probe analysis. Aluminum and Graphite materials were used for the hollow cylinder target and optical diagnostics revealed the ion charge states present in the dense plasma cloud inside the hollow cylinder. For the aluminum target, singly charged aluminum ions were identified from the optical emission lines of the plasma and traces of iron, carbon and oxygen could also be detected. The graphite target however showed high charge state carbon ions of up to +3. Aside from the emission lines, a continuum was observed in the optical emission spectra which indicates a thermalization occuring in the plasma and the plasma temperature could be estimated to be below 1 eV. Langmuir probe experiments were also conducted to estimate the electron temperature which was calculated to be 0.48 eV which is in the same order of temperature observed through the optical emission spectra. This concludes the first version of the system design.

In chapter five, the next phase of the development process of the laser ion source was to assess the stability and reproducibility. The laser ion source operated using a stationary hollow target which had fluctuating ion signals and a short target lifetime from surface erosion due to laser irradiation. The addition of a rotational mechnism allowed the inner walls to be evenly eroded radially maintaining stability and extended the lifetime of the target to more than 1 hour. Faraday cup measurements of aluminum and graphite targets using the rotational system design compared the plasma conditions between the two materials. The current intensity of the aluminum target was observed to be higher than the graphite target but the plasma temperature was found to be higher for the carbon plasma.

In chapter six, with the stable operation of the laser ion source, the ion species generated from the plasma were determined through mass analysis experiments. Two mass analyzer experiments were performed, one is by electrostatic acceleration

coupled to a time-of-flight analysis and the other is by a 90° deflection through an electrostatic ion analyzer.

The ion acceleration through electrostatic forces extracted the laser produced ions and the mass separated ion signals were detected by a Faraday cup. The graphite target showed signals for singly charged carbon ions including C^{+2} and C^{+3}. Slow and massive ion signals were also detected in the measurement indicating the formation of carbon clusters of C_2, C_4, C_{16}, including small fullerites of C_{24}, and C_{36}. For the ion extraction of the plasma formed using an aluminum target, singly charged aluminum ions were detected. Aluminum clusters of Al^{+3} and Al^{+5} were identified from the time-of-flight measurements including slow ion signals that correspond to large clusters of Al_{20} and Al_{52}. Since the ions coming from the plasma has initial kinetic energy obtained from the self-induced acceleration field by the charge separation during diffusion, the energy was deduced through the arrival time of the ion signals from the time-of-flight. For singly charged aluminum and carbon ions, the initial kinetic energy was revealed to be identical at 0.5 eV.

For the 90° electrostatic ion analyzer, the relation between the drift distance and the ion peak intensity needed to be evaluated first. Space resolved Faraday cup measurements at distances 60 cm to 90 cm were obtained and a fitting curve verified the validity of the relation $I_p \alpha L^{-3}$ where L is the drift distance. This permitted the estimation of the ion composition analysis by the electrostatic ion analyzer. The positive ions generated from the plasma were carbon ions of up to +3 charge states and the presence of H^+ that originated from monolayer adsobrates of hydrogen. The current profile from the Faraday cup was compared to the mass separated ion signals and the composition of the plasma pulse was acquired from the analysis. The ions in a single plasma pulse was mainly dominated by C^{+1} and C^{+2} ions and a small portion of H^+ and

C^{+3} contributed to the initial part of the current distribution with the light and energetic particles arrive fastest. The abundance of low charge state ions C^{+1} and C^{+2} suggests the low energy in the plasma enabling only the formation of up to a minimum amount of C^{+3} ions.

Based on the experiments during the development of the hollow cylinder target laser ion source, a low plasma temperature condition was caused by the geometric constriction of the target on the expanding plasma plume. This important point was an indication of the suitable condition for atomic agglomeration leading to the formation clusters as observed in the mass separated ion analysis experiments. Utilizing geometric structures for spatially confining the plasma is a key technique for transforming the laser ion sources for cluster ion production.

7.2 The New Target Structure

The operation of the laser ion source with a hollow cylinder target has changed the plasma dynamics of the laser produced plasma. A conventional laser ablation setup uses a planar target for production of particle flux and the expansion process is unobstructed as it drifts outward. For the case of the hollow cylinder target, the plasma is ignited inside the cylinder and interacts with the inner walls of the target as the plasma exits out of the structure. The two expansion dynamics have differences that are observed in the experiments.

First, the laser energy required to produce the signals for the hollow cylinder target was higher because the plasma needs to build pressure inside the hollow volume before flowing out of the target. For the Faraday cup measurements, the laser ablation using an aluminum target exhibited a steep rise in the ion current profile which was indicated

by the amount of energetic in the plasma pulse but broader with a lower magnitude for low laser power. The mass separated ion signals also showed aluminum ions of up to +3 charge states with their proportional to the laser power density. Comparing the signals to the hollow cylinder target, the current profiles were similar in form but the mass analysis experiments, however, showed the presence of slow and massive ions. The very slow ion signals could not be detected in the planar target since this is a direct effect of the geometric constriction. Higher charge state ions were not detected in the ions signals for the hollow cylinder target which confirms the energy dissipation creating the condition for low charge state ions and the formation of neutrals through the increased collision rate.

7.3 Future Work

The research work on utilizing the hollow cylinder target in a laser ion source has showed the cluster ion formation in the spatially bound plasma. Although the operation of the ion source was demonstrated, there are few operational issues that needs to be addressed as well as recommendations for future work.

The propagation of the laser produced plasma can be investigated more in detail to verify the preferential direction of the ion trajectory. This is essential for the design of an extraction system and additional beam diagnostics like magnetic mass analyzers for the ion source. The cluster ion formation in the laser ion source can be analyzed further to develop the system as a cluster ion source. The current hollow cylinder design experiences a backflow of the expanding plasma. Modifications to the cylindrical design such as a tapered structure can minimize the beam loss and improve the performance

of the system. Different target designs can also be explored to observe the changes in the plasma expansion dynamics with spatial obstructions.

Since the laser ion source has been the first attempt to utilize a hollow cylinder laser target, there are many aspects to improve the system to reach a certain degree of success in its performance as an ion source.

References

[1] N. J. Peacock and R. S. Pease, J. Phys. D 2, 1705 (1969).

[2] G. Francis, D. W. Atkinson, P. Avivi, J. E. Bradley, C. D. King, W. Millar, P. A. H. Saunders, A. F. Taylor, Phys Lett. 25 A, 486 (1967).

[3] J. Tamura, M. Okamura, T. Kanesure, S. Kondrashev, Appl. Phys. Lett. 91, 041504 (2007).

[4] P. Yeates, J. T. Costello, E. T. Kennedy, Rev. Sci. Instrum. 81, 043305 (2010).

[5] N. Munemoto, K. Takayama, S. Takano, M. Okamura, M. Kumaki, Rev. Sci. Instrum. 85, 02B922 (2014).

[6] H. Y. Zhao, Q. Y. Jin, S. Sha, J. J. Zhang, Z. M. Ki, W. Lie, L.T. Sun, X. Z. Zhang, H. W. Zhao, Rev. Sci. Instrum. 85, 02B910 (2014).

[7] M. Sekine, S. Ikeda, M. Romanelli, M. Kumaki, Y. Fuwa, T. Kanesue, N. Hayashizaki, R. Lambiase, M. Okamura, Nucl. Instrum. Methods Phys. Res. A. 795, 151-155 (2015).

[8] T. Kanesue, Y. Fuwa, K. Kondo, M. Okamura, Appl. Phys. Lett. 105, 193506 (2014).

[9] Y. Fuwa, S. Ikeda, M. Kumaki, M. Sekine, D. Cinquegrani, M. Romanelli, T. Kanesue, . Okamura, Y. Iwashita, Rev. Sci. Instrum. 85, 02B916 (2014).

[10] M. Sekine, S. Ikeda, N. Hayashizaki, T. Kanesue, M. Okamura, Rev. Sci. Instrum. 85, 02B920 (2014).

[11] A. Bialous, M. Gazda, K. Growchowska, P. Atanasov, A. Dikovska, N. Nedyalkov, J. Reszczynska, A. Zaleska-Medynska, G. Sliwinski, Thin Solid Films. 601, 41-44 (2016).

[12] A. Di Berardo, C, Courtois, B. Cros, G. Matthieussent, D. Batani, T. Desai, F. Strati, G. Lucchini, Laser Part. Beams. 21, 59-64 (2003).

[13] G. Muñoz, P. Homm, F. Guzman, H.M. Ruiz, L.S. Caballero, M. Favre, M. Flores, and S. Hevia, J. Phys: Conf. Ser. 591, 012047 (2015).

[14] C. Phipps, Laser Ablation and its Applications (Springer Series in Optical Sciences, 2007).

[15] A. Bogaerts, Z. Chen, Spectrochim. Acta, Part B. 60, 1280-1307 (2005).

[16] M. Stafe, A. Marcu, N. Puscas, Pulsed Laser Ablatioin of Solids (Springer Series in Surface Sciences, 2014).

[17] N.M. Bulgakova, A.V. Bulgakov, Appl. Phys. A. 73, 199-208 (2001).

[18] S.I. Anisimov, D. Bauerle, B.S. Luk'yanchuk, Phys. Rev. B. 48, 16 (1993).

[19] R. K. Singh, J. Narayan, Phys. Rev. B. 41, 13 (1990).

[20] I. G. Brown, The Physics and Technology of Ion Sources (Wiley, New York, 2005).

[21] W.L. Bohn, Proc. SPIE 7005, High-Power Laser Ablation VII, 70051C (2008).

[22] X. Wang, S. Zhang, X. Cheng, E. Zhu, W. Hang, and B. Huang, Spectrochim. Acta B 99, 101 (2014).

[23] H. Togashi, K. Saito, Y. Koga, H. Yamawaki, K. Aoki, M. Mukaida, T. Kameyama, Appl. Surf. Sci. 96-98, 267-271 (1996).

[24] E. Cappelli, C. Scilletta, G. Mattei, V. Valentini, S. Orlando, M. Servidori, Appl. Phys. A: Mater. Sci. Process. 93, 751-758 (2008).

[25] T. Fujimoto, Plasma Spectroscopy (Clarendon Press, Oxford, 2004) pp.30-48.

[26] C. Kittel, H. Kroemer, Thermal Physics (W.H. Freeman and Company, New York, 1980) 2nd ed. pp.91-98.

[27] O. Auciello, D. L. Flamm, Plasma Diagnostics Vol. 1 (Academic Press, UK, 1989) pp. 1-46.

[28] Trubnikov, Particle interactions in a fully ionized plasma, in: M.A. Leontovich (Ed.), Review of Plasma Physics Vol. 1, Consultants Bureau, New York, 1965, pp. 172-174.

[29] T. Forrester, Large Ion Beams: fundamentals of generation and propagation (Wiley, US, 1988) pp.85-96.

[30] R. Kelly, R. Dreyfus, Surf. Sci. 198, 1, 263-276 (1988).

[31] Y. P. Raizer, Gas Discharge Physics (Springer-Verlag, Germany, 1991).

[32] F. F. Chen, Introduction to Plasma Physics (Plenum Press, New York, 1974).

[33] L. Spitzer, Physics of Fully Ionized Gases (Wiley Inter-science, New York, 1962).

[34] B. Doggett and J. G. Lunney, J. Appl. Phys. 109, 093304 (2011).

[35] D. Doria, A. Lorusso, F. Belloni, V. Nassisi, L. Torrisi, and S. Gammino, Laser Part. Beams, 22, 461-467 (2004).

[36] F. J. Gordillo-Vazquez, A. Perea, J. A. Chaos, J. Gonzalo, and C. N. Afonso, Appl. Phys. Lett. 78, 7-9 (2001).

[37] A. Yamaguchi, K. Sako, K. Sato, N. Hayashizaki, and T. Hattori, Rev. Sci. Instrum. 85, 02B921 (2014).

[38] J. Akola, H. Hakkinen, and M. Manninen, Phys. Rev. B 58, 7, 3601-3604 (1998).

[39] T. Kobayashi, Y, Matsuo, Appl. Phys. B 119, 435-438 (2015).

[40] S. Sonntag, C. Trichet Paredes, J. Roth, H. R. Trebin, Appl. Phys. A 559-565 (2011).

[41] M. Bacal, M. Wada, Appl. Phys. Rev. 2, 021305 (2015).

[42] M. Okamura, T. Takeuchi, R. A. Jameson, S. Kondrashev, H. Kashiwagi, K. Sakakibara,

[43] T. Kanesue, J. Tamura, and T. Hattori, Rev. Sci. Instrum. 79, 02B314 (2008).

[44] D. Tomanek, and M. Schluter, Phys. Rev. Lett. 67, 17, 2331-2334 (1991).

[45] S. Sha, H. W. Zhao, X. H. Guo, Z. L. Zhang, X. Fang, J. W. Guo, W. H. Zhang, W. Lu, Y. Cao, H. Y. Ma, S. H. Lin, X. X. Li, B. H. Ma, Y. Yang, H. Wang, Q. Wu, J. Y. Li, Y, C, Feng, H. Y. Zhao, Y. H. Zhu, L. T. Sun, x. Z. Zhang, X. M. Chen, and D. Z. Xie, Rev. Sci. Instrum. 83 02B303 (2012).

[46] A. Y. Wong, J. M. Dawson, W. Gekelman, and Z. Lucky, Appl. Phys. Lett. 25, 10, 579-580 (1974).

[47] S. Ikeda, M. Romanelli, D. Cinquegrani, M. Sekine, M. Kumaki, Y. Fuwa, T. Kanesue, M. Okamura, and K. Horioka, Rev. Sci. Instrum. 85, 02B919 (2014).

[48] R. Tuckfield, and F. Schwirzke, Plasma Physics, 44, 1, 11 (1969).

[49] S. S. Harilal, M. S. Tillack, B. O'Shay, C. V. Bindhu, and F. Najmabadi, Phys. Rev. E 69, 026413 (2014).

[50] M. Okamura, M. Sekine, K. Takahashi, K. Kondo, and T. Kanesue, Nucl. Instrum. Methods Phys. Res. A. 733, 97-102 (2014).

[51] J. C. S. Kools, T. S. Baller, S. T. De Zwart, and J. Dieleman, J. Appl. Phys. 71, 9, 4547-4556 (1992).